CHAPTER 6

Development and Modeling of Solar Photocatalytic Reactors

Camilo A. Arancibia-Bulnes*, **Antonio E. Jiménez,** and **Claudio A. Estrada**

Contents

Centro de Investigación en Energía, Universidad Nacional Autónoma de México, Privada Xochicalco s/n, Col. Centro, A. P. 34, Temixco, 62580 Morelos, México

* Corresponding author.
E-mail address: caab@cie.unam.mx

Advances in Chemical Engineering, Volume 36
ISSN 0065-2377, DOI: 10.1016/S0065-2377(09)00406-2

1. INTRODUCTION

Photocatalysis is an advanced oxidation process with a high potential for the treatment of water contaminated with persistent organic pollutants. In this process ultraviolet radiation is used for the excitation of a semiconductor catalyst (usually TiO_2) in contact with the polluted water. When photons are absorbed by the catalyst electrons are promoted to the conduction band, leaving holes in the valence band. These charges can diffuse to the surface of the material where they initiate oxidation/reduction reactions with molecules adsorbed in the semiconductor surface. Due to the high cost and environmental impact of the utilization of artificial UV light in photocatalytic processes, there has been a great deal of interest in the application of solar energy. Other advanced oxidation processes able to use solar energy, particularly photo-Fenton, are also very interesting but will not be considered in this review due to the space limitations.

In solar photocatalytic detoxification of water, as in any other solar energy application, the adequate design and sizing of systems is of the greatest importance. As the solar resource is relatively diluted, the need to invest in large collector fields is a major factor affecting the final cost per unit product. This is particularly true for photocatalysis, where only a fraction of the solar radiation spectrum can be utilized. Therefore, the design of solar photoreactors should be aimed at making the best use of the available UV solar radiation.

Solar photoreactors are often classified into nonconcentrating and concentrating, depending on whether they operate with solar radiation as it arrives to earth's surface or use a solar concentrator to augment the radiative flux impinging on the reactor. From the basic mechanisms of photocatalysis it is well known that the kinetics of reactions behaves linearly with the radiation intensity when this intensity is low, and as the square root when this intensity is high. As a consequence of this, nonconcentrating reactors make a more efficient use of solar radiation, although concentrating reactors are faster. Because of this, recent research has focused mostly on the former and on reactors with low concentration factors, particularly those based on compound parabolic collectors (CPC). These types of reactors have also been used for the disinfection of water.

Another area which has gained interest in recent years is the utilization of supported catalyst in solar photoreactors, as opposed to suspended catalyst. Different geometries have been proposed for supporting the catalyst, which are strongly linked to photoreactor geometry. Results have been in some cases very good, despite of the fact that traditionally suspended catalyst has been considered more effective.

The modeling of radiation absorption within solar photocatalytic reactors has been addressed by some researchers, but is one of the areas where less work has been carried out. Both heuristic and first principles methods,

based on the radiative transfer equation (RTE), have been used. This is linked also with the utilization of kinetic models based on the radiation absorbed by the catalyst, as opposed to models based only on radiation arriving to the solar collector.

In some cases, evaluating a global reaction rate based on the total radiation absorbed by the reactor is not equivalent to evaluate rates based on the radiation absorbed locally, especially when mass transfer limitations occur. Thus, appropriate analysis of radiative transfer in reactors can be a valuable tool in making design decisions.

2. SOLAR PHOTOCATALYTIC REACTORS

In solar photocatalytic reactors the source of the photons necessary to carry out the excitation of the catalyst is near-UV solar radiation. This implies that two optical problems have to be dealt with in the design of these reactors: (1) to collect solar radiation, and (2) to distribute this radiation in the best possible manner inside the reaction volume. These tasks should be done with the highest possible efficiency, as the amount of solar energy available in the wavelength range utilizable by TiO_2 is small. The work in solar photocatalytic reactors has been reviewed in several works (Alfano et al., 2000; Bahnemann, 2004; Blanco-Galvez et al., 2007; Goslich et al., 1997; Goswami, 1995, 1997; Goswami et al., 2000; Malato et al., 2007; Malato Rodríguez et al., 2004), so our aim here is only to discuss the main ideas and to review some recent work.

2.1. Solar reactor types

Different types of solar photocatalytic reactors have been developed over time. Two main distinctions have been made: (i) concentrating versus non-concentrating reactors and (ii) slurry versus fixed catalyst reactors. These two classifications are not mutually exclusive, and other categories may also be established, for instance, a very important is the one of tubular solar photoreactors.

Let us start by pointing out some characteristics of solar radiation which affect the design of photoreactors, as one may try to make an optimal use of the available radiation. First of all, the usable solar radiation is restricted by two factors: on the one hand, the fact that solar radiation at the earth's surface starts at wavelengths larger than 300 nm. On the other hand, that the most common semiconductor used in photocatalysis is anatase TiO_2. Because of the magnitude of its energy band gap, small particles of this material absorb radiation very poorly for wavelengths above 370 nm. Many attempts to develop catalysts with a more extended spectral response have been done, but they have failed to date to provide a low-cost alternative

(Blanco-Galvez et al., 2007). Thus, the usable wavelengths barely coincide with the solar UV range (from 300 to 400 nm). This means that the radiation available to carry out photocatalytic reactions is around 5% of the global solar radiation; that is, at most 50 $W\,m^{-2}$ (Hulstrom et al., 1985).

A second characteristic of UV solar radiation is that, even for very clear atmospheres, it is composed in similar amounts of both beam and diffuse radiation (Hulstrom et al., 1985). The first is defined as the radiation arriving directly from the sun, while the second is the solar radiation that has been scattered by gases and aerosols after entering the earth's atmosphere. This second type of radiation reaches the ground in a more or less diffuse manner; that is, with similar intensity from all directions in the sky. In this respect, the situation encountered in solar photocatalytic reactors is quite different from the one encountered in solar thermal collectors. The latter are able to use the whole solar spectrum, and in that case diffuse radiation accounts for a much smaller fraction of the global irradiance.

The solar concentration ratio of a solar collector is defined as the ratio of the aperture area of the reflector to the area of the receiver (Rabl, 1985). This quantity gives an approximation to the number of times the radiative flux density ($W\,m^{-2}$) is increased in the surface of the receiver, as compared to the incoming solar radiation. The concentration ratio is commonly expressed as a number of "suns"; for instance, a collector that increases the radiative flux density five times is said to have a five suns concentration ratio. Thus, the formula for the concentration ratio is

$$C_R = \frac{A_a}{A_r} \tag{1}$$

The first type of photocatalytic reactors employed were parabolic trough concentrators (PTC) with one- or two-axis tracking systems to follow the apparent movement of the sun in the sky. These photocatalytic reactors were just standard medium concentration ($C_R \approx 15$ suns) thermal collectors, which were readily adapted as photocatalytic reactors by replacing the absorber tube by a Pyrex glass tube (Alpert et al., 1991; Minero et al., 1993) (Figure 1). However, it was eventually found that PTC reactors had several disadvantages which made them energetically less efficient and more expensive than nonconcentrating reactors (Malato et al., 1997):

1. Concentrating collectors are only able to use a limited fraction of the diffuse solar radiation. This utilizable fraction can be estimated as the inverse of the concentration ratio of the collector ($1/C_R$) (Rabl, 1985). Because of this, parabolic trough photocatalytic reactors, which have a concentration ratio around 15 or higher, miss practically all diffuse radiation. This amounts to losing around half of the available UV solar irradiance.

Figure 1 Parabolic trough photocatalytic reactor at Plataforma Solar de Almería (reprinted from Malato et al., 2007 with permission from Elsevier).

2. Reaction rates in photocatalysis have been observed to be proportional to the square root of radiation intensity, at medium and high concentration levels (see Section 2.3). Thus, nonconcentrating reactors make a more efficient use of the collected photons. In the end, this diminishes the total collector area required as compared to concentrating reactors.
3. Medium and high concentrating reactors require tracking systems that are costly, require maintenance, and consume energy.
4. Concentration may lead to overheating of the water and evaporation, especially when dealing with nontransparent pollutants as dyes.

Nevertheless, PTC reactors do have some attractive features. First of all, they allow the degradation of pollutants at faster rates (although with larger collector areas), simply by delivering more photons per unit volume in the reaction space. Also, tracking helps to make a more efficient use of the beam UV radiation component along the entire day by keeping the collector aperture normal to the sun rays.

In parallel with the experiences with PTC reactors, the development of several types of nonconcentrating reactors was pursued by different research groups. Among nonconcentrating photoreactors we can mention, falling film reactors (Bockelmann et al., 1995; Gernjak et al., 2004) (Figure 2), the shallow pond reactor (Bedford et al., 1994), the flat tubular photoreactors (Goswami, 1997), flat plastic reactors (van Well et al., 1997), multistep

Figure 2 Thin film fixed bed reactor (reprinted from Bahnemann, 2004, with permission from Elsevier).

cascade falling-film reactors (Guillard et al., 2003; Pichat et al., 2004), and reactors based in CPC (Blanco et al., 1999) (Figure 3). On the other hand, some researchers have even used systems with higher concentration ratio than PTC (Oyama et al., 2004).

In particular, nonconcentrating CPC reactors are currently regarded as one of the best options for large-scale applications of solar photocatalysis, because they combine some advantages of both PTC and nonconcentrating reactors (Malato Rodriguez et al., 2004) as follows:

1. They are able to collect both beam and diffuse solar radiation.
2. They have low fabrication costs as compared to PTC, mainly because they do not require sun tracking systems.
3. They use a closed tubular reaction space as receiver, like PTC, and this helps avoiding the evaporation of volatile compounds.
4. They withstand more pressure than other reactors due to the tubular geometry of the flow space. This allows working in the turbulent regime.
5. They avoid water overheating.

It is important to point out that most of these advantages are also shared by other nonconcentrating tubular reactors. However, the optical efficiency of CPC is near to the theoretical maximum (Rabl, 1985), as will be discussed

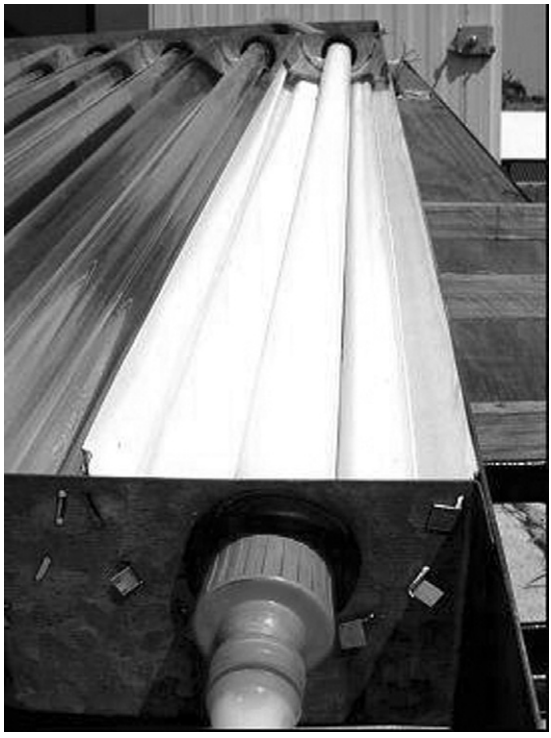

Figure 3 CPC photoreactor (developed by AoSol, Portugal).

in the next section. This is not so for other nonconcentrating tubular collectors (TC), which miss some amounts of diffuse and beam radiation depending on the incidence angle.

As stated previously, another distinction usually made is between slurry and supported catalyst reactors. In slurry photocatalytic reactors the catalyst is present in the form of small particles suspended in the water being treated. These reactors generally tend to be more efficient than supported catalyst reactors, because the semiconductor particles provide a larger contact surface area per unit mass. In fact, the state of the photocatalyst is important both to increase contaminant adsorption and to improve the distribution of absorbed radiation. In a slurry unit the photocatalyst has a better contact with the dissolved molecules and is allowed to absorb radiation in a more homogeneous manner over the reaction volume. Using suspended catalyst has been the usual practice in PTC, CPC, and other types of tubular reactors. The drawback of this reactor design is the requirement for separation and recovery of the very small particles at the end of the water treatment process. This may eventually complicate and slow down the water throughput.

Given this situation, the use of supported photocatalyst has attracted significant research efforts. Several ways have been proposed to support the semiconductor, such as coating of extended surfaces (Diaz et al., 2007; Gryglik et al., 2004) or glass beads (Gelover et al., 2004). In the first case, photocatalytic reactors are designed with shallow depths to ensure proper illumination of the supported semiconductor. For instance, this is the case of the thin film fixed bed reactor (Bockelmann et al., 1995) or multistep cascade reactor (Guillard et al., 2003).

Supporting the catalyst on beads gives more flexibility to reactor geometry than doing it on extended surfaces. It has been observed in some cases that reactors with TiO_2-coated glass beads can reach efficiencies similar to slurry photoreactors. For instance, Gelover et al. (2004) deposited anatase thin films over small cylindrical pieces of glass, using a sol–gel technique. They carried out the degradation of 4-chlorophenol and carbaryl in a PTC in which the tubular reaction space was filled with these glass pieces. The results obtained with this configuration were compared to results obtained in the same reactor when suspended catalyst was used. Similar degradation rates were observed in both cases.

Besides the applications for detoxification, in recent years the catalyst support geometry and its optimization have also been investigated for application in water disinfection (see, for instance, McLoughlin et al., 2004a; Meichtry et al., 2007; Navntoft et al., 2007).

2.2. CPC photoreactors

As discussed in the previous section, one type of solar collector geometry that has been found to be very advantageous for solar photocatalysis is based on CPC (Blanco et. al., 1999), which are a type of nonimaging optical devices.

A common classification for solar collectors is between imaging and nonimaging collectors. The first are based on optical designs originally intended for imaging applications; that is, they are able to produce an image of the radiation source (the sun) in their focal region. For instance, this is the case of PTC, which are able to produce a two-dimensional image of the sun over a flat receiver.

The requirement of producing an image of the source imposes serious limitations in the capacity of optical systems for collecting light. Nonimaging solar collectors are freed from these constraints in order to reach better energetic performance. In this kind of optical systems the goal is reaching the maximum possible capture of light over a given collection angle, which is called acceptance half angle θ_{max}. Thus, light rays arriving to the system's aperture within the acceptance angle are ensured to reach the receiver, regardless of the fact that they may not produce an image of the source (Figure 4).

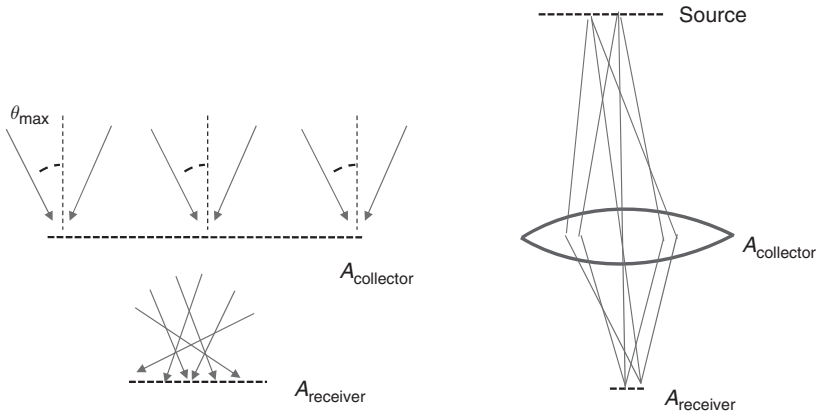

Figure 4 Nonimaging (left) versus imaging (right) optical systems. In the latter all light rays coming from a point in the source must be imaged to a point in the receiver.

Due to the relaxation of the requirement to form images, some nonimaging collectors, called ideal collectors, are able to reach the maximum possible collection of light for a given concentration ratio. In particular, the maximum concentration ratio of line focusing solar collectors is given by (Rabl, 1976, 1985; Winston et al, 2005)

$$C_{R,max} \leq \frac{1}{\sin \theta_{max}} \tag{2}$$

The interpretation of Equation (2) is that if a solar collector is to be able to capture all of the radiation incident within the acceptance cone defined by θ_{max} (Figure 4), at most it can have a concentration ratio given by C_{max}. This rule comes from the fundamental principles of thermodynamics (Rabl, 1985) and is obeyed by all optical systems.

The other way of looking at Equation (2) is that, for a given concentration ratio, an ideal collector is able to collect radiation over the widest possible angle. CPC may be designed in principle to have different concentration ratios, depending on their acceptance angle. In particular, nonconcentrating CPC ($C_R \approx 1$) used in photocatalysis are able to collect radiation from the whole hemisphere ($\theta_{max} = \pi/2$) (Blanco et al., 1999), being this their main advantage over other nonconcentrating tubular reactors.

Originally, the term CPC was coined to refer to a concentrator consisting of two parabolic segments rotated relative to each other. This kind of geometry was designed specifically to concentrate radiation in a planar absorber. However, the designation CPC has evolved to include other kinds of nonimaging solar concentrators (Winston et al., 2005). For instance, in the case of a tubular receiver the ideal reflector is usually called a CPC,

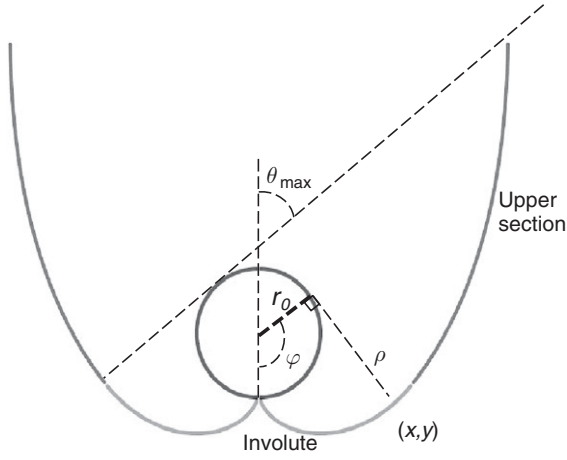

Figure 5 Geometry of a CPC for a tubular receiver.

but is formed by two involute sections instead of two parabolas. For concentrations higher than unity these involute sections are continued by segments that are also not parabolic (Figure 5).

The following are the equations of a CPC for a tubular receiver (Rabl, 1985): the coordinates of the points of the concentrator are given in a parametric form by

$$x = r_0 \sin\varphi - \rho\cos\varphi \tag{3}$$

$$y = -r_0\cos\varphi - \rho\sin\varphi \tag{4}$$

with φ a polar angle around the tubular receiver of radius r_0, as presented in Figure 5. For the involute (lower) section of the concentrator this angle is bound as $0 \le \varphi \le \pi/2 + \theta_{\max}$ and the distance ρ is given by

$$\rho = r_0\,\varphi \tag{5}$$

For the upper section of the concentrator φ is restricted to the range $\pi/2 + \theta_{\max} \le \varphi \le 3\pi/2 - \theta_{\max}$, and

$$\rho = r_0\,\frac{\pi/2 + \theta_{\max} + \varphi - \cos(\varphi - \theta_{\max})}{1 + \sin(\varphi - \theta_{\max})} \tag{6}$$

In particular, in nonconcentrating CPC only the involute part of the reflector is used with φ up to π (see, for instance, Figure 3).

As it can be observed in Figure 5, the upper part of a CPC consists of a large reflector area that is nearly vertical, and which adds very little to the

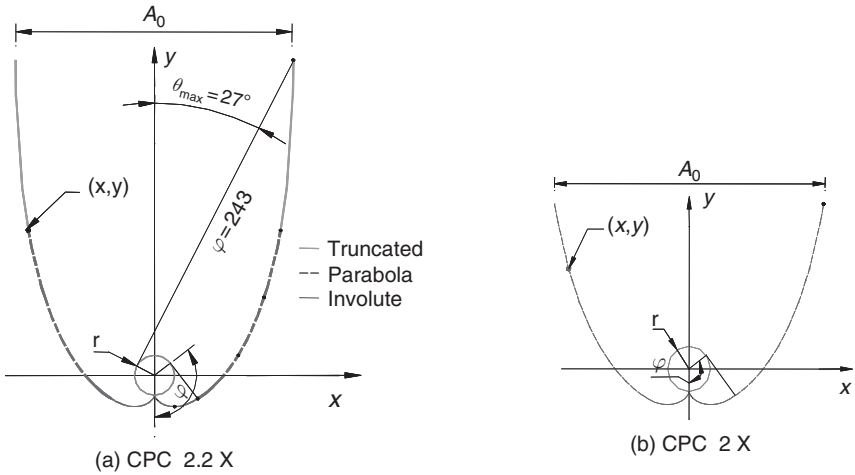

Figure 6 Truncation of a 2.2 suns CPC (a), to 2 suns (b) (Jiménez and Salgado, 2008).

aperture area A_a. Therefore, this part of the concentrator can be heavily truncated without reducing significantly the concentration ratio (Carvalho et al., 1985). For instance, Figure 6 illustrates the truncation of a CPC with 2.2 suns concentration ratio. With this operation, around 50% of the reflecting material is saved, but the collector loses only about 10% concentration ratio.

It is important to point out that Equations (3)–(6) are only valid for CPC with tubular receivers. Nevertheless, the methods of nonimaging optics (Winston et al., 2005) allow the design of CPC reflectors for receivers of varied geometry. For instance, Chaves and Collares Pereira (2007) proposed a design of a CPC with a vertical stripe of supported catalyst as receiver (fin). This fin is contained in the water phase (Figure 7) inside a glass tube. This illustrates how, as new geometries for catalyst support are studied, consideration should be paid to the optimal design of the required reflectors.

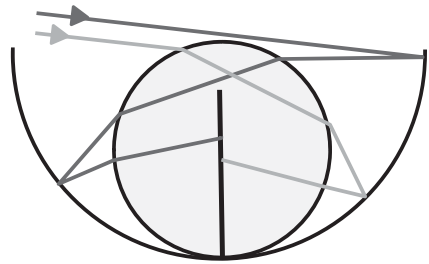

Figure 7 CPC reflectors for a tubular reactor with catalyst supported in a vertical stripe. Adapted from Chaves and Collares Pereira (2007), with permission from The American society of Mechanical Engineers.

2.3. The dependence of reaction rates on radiation intensity

Radiation absorption is the initiating step in photocatalytic processes. When a photon of energy greater than the band gap of the semiconductor catalyst arrives to its surface, it is absorbed and promotes an electron from the valence to the conduction band, creating an electron–hole pair. Therefore, the quantity of interest is the number of photons absorbed by the catalyst, characterized in a slurry photoreactor by the so-called local volumetric rate of photon absorption (LVRPA). This quantity is the number of photon mol (Einstein) absorbed in the suspension per unit volume and time. Taking into account that the energy of a photon of wavelength λ is given by $E_\lambda = hc/\lambda$, where h is Planck's constant and c is the speed of light, the LVRPA is obtained in terms of the power absorbed by the catalyst at each wavelength

$$e_{\mathrm{L}}(\mathbf{r}) = \frac{1}{hcN_{\mathrm{A}}} \int Q^{m}_{\mathrm{abs-cat},\lambda}(\mathbf{r})\ \lambda\, \mathrm{d}\lambda \tag{7}$$

Here e_{L} is the LVRPA, N_{A} is Avogadro's number, and $Q^{m}_{\mathrm{abs-cat},\lambda}$ is the volumetric power absorbed by the catalyst (see Section 3.2) at a given point $\mathbf{r}$ in the reactor volume and per unit wavelength. This integral is carried out over the wavelength range defined by the intersection of the spectrum of the radiation source, with the absorption region of the catalyst. In the case of solar radiation and TiO_2 catalyst this region is usually considered to be from 0.3 to 0.4 μm.

The relationship between the local reaction rate and the LVRPA can be obtained from models of the reaction mechanism. By considering the steps proposed by Turchi and Ollis (1990), and taking into account the simplifications proposed by Bandala et al. (2004), it is obtained

$$\frac{\mathrm{d}C_{\mathrm{p}}(\mathbf{r})}{\mathrm{d}t} = \frac{-k_\alpha k_{\mathrm{F}}\, C_{\mathrm{p}}(\mathbf{r})\, (-1+\sqrt{1+\gamma^2 e_{\mathrm{L}}})}{k_\alpha C_{\mathrm{p}} + k_{\mathrm{O},1}[R_1] + k_{\mathrm{O},2}[R_2] + \cdots + k_{\mathrm{O},n}[R_n]} \tag{8}$$

where

$$\gamma = \frac{4k_{\mathrm{e}}k_{\mathrm{R}}}{k_{\mathrm{F}}k_{\mathrm{E}}} \tag{9}$$

The local concentration of the pollutant is denoted by $C_{\mathrm{p}}(\mathbf{r})$. This concentration depends on the position inside the reactor (denoted by vector $\mathbf{r}$), unless perfect mixing is attained. The quantities $[R_1]$, $[R_2]$, $[R_n]$ are the concentrations of possible intermediate compounds. k_α, k_{F}, $k_{\mathrm{O},1}$, $k_{\mathrm{O},2}$, $k_{\mathrm{O},n}$, k_{e}, k_{R}, k_{F}, and k_{E} are kinetic constants for the different steps involved in the photocatalytic process (Alfano et al., 1997; Bandala et al., 2004; Turchi and Ollis, 1990).

The above equation gives the local reaction rate as a product of two functions, one dependent on the concentration of the pollutant and the intermediates only, and a second one dependent only on the LVRPA. Note that all the concentrations are location dependent as well as e_L. To obtain the evolution of the average concentration of the pollutant it is necessary to average Equation (8) over the suspension volume V_T

$$\frac{dC_{p,av}}{dt} = \frac{1}{V_T}\int_{V_T} F_1(C_p, [R_i])\, F_2(e_L)\, dV \tag{10}$$

where, from Equation (8), the functions F_1 and F_2 are defined as

$$F_1(C_p, [R_i]) = \frac{-k_\alpha k_F\, C_p(\mathbf{r})}{k_\alpha C_p + k_{O,1}[R_1] + k_{O,2}[R_2] + \cdots + k_{O,n}[R_n]} \tag{11}$$

$$F_2(e_L) = -1 + \sqrt{1 + \gamma^2 e_L} \tag{12}$$

Note that while it is often possible to improve mixing in order to have pollutant concentrations that are not site dependent, it is generally not possible to have a homogeneous value for the LVRPA. Therefore the above equation can be expressed as

$$\frac{dC_{p,av}}{dt} = F_1(C_{p,av}, [R_i])\frac{1}{V_T}\int_{V_R} F_2(e_L)\, dV \tag{13}$$

In this equation the integration should be restricted to the irradiated section (the photoreactor) of volume V_R. In the dark parts of the system the second function is zero. However, it must be pointed out that when important mass transfer limitations occur Equation (13) is no longer valid. For instance, Ballari et al. (2008) found that this may be the situation under conditions of high catalyst loading and high irradiation rates.

The determination of the distribution of the LVRPA requires the use of some type of radiative transfer model. In the case of transparent pollutants, it can be considered that e_L depends on TiO_2 concentration (C_{catal}) only, and not on the concentration of the pollutant, since it is the former component which absorbs and scatters radiation. This allows uncoupling the radiation problem from the degradation kinetics when Equation (13) is solved; that is, one can first evaluate e_L and then, independently of the value of the pollutant concentration, integrate $F_2(e_L)$ over the reactor volume. Once this quantity has been calculated, its numerical value is taken as a constant in Equation (13), which can now be solved to obtain the evolution of $C_{p,av}$.

For Equation (12) there are two limit cases at high and low solar radiation concentrations, respectively

$$F_2(e_L) \cong \gamma\sqrt{e_L} \quad \text{if} \quad \gamma^2 e_L \gg 1 \tag{14}$$

$$F_2(e_L) \cong \left(\frac{\gamma^2}{2}\right) e_L \quad \text{if} \quad \gamma^2 e_L \ll 1 \tag{15}$$

These equations mean that a linear dependence of the reaction rate with light intensity (LVRPA) is observed when intensities are small, while square root dependence is observed when intensity is high. This latter dependence occurs for high intensities because the recombination of electron–hole pairs starts to limit the efficient use of the available photons (Alfano et al., 1997). The intensity at which the crossover between these two types of behavior occurs depends on the value of the lumped kinetic parameter γ, which in turn depends on the specific reaction under consideration.

The above theoretical expressions coincide with the experimental observations. Bahnemann et al. (1991) carried out the photocatalytic degradation of chloroform, varying radiation intensities by five orders of magnitude. They found a nonlinear correlation between the degradation rate and radiation intensity. Similarly, studies of phenol degradation carried out by Okamoto et al., (1985) showed a square root relationship between degradation rate and intensity. Nevertheless, at small intensities a linear relationship is observed. For instance, Román Rodríguez (2001) studied the solar photocatalytic degradation of carbaryl with concentration ratios up to five suns and observed this linear relationship.

For nonabsorbing substrates, a factor can be defined that takes into account the effect of all the optical processes in the reaction rate. This factor has been called reaction rate optical factor (RROF) (Arancibia-Bulnes and Cuevas, 2004)

$$R_{opt} = \int_{V_R} \left(-1 + \sqrt{1 + \gamma^2 e_L}\right) dV \tag{16}$$

For small values of γ, when the kinetics is linear with respect to the LVRPA, this integral increases asymptotically with catalyst concentration (Arancibia-Bulnes and Cuevas, 2004). However, when square root dependence dominates, this factor reaches a maximum and then starts to decrease with increasing catalyst concentration. This means that too much catalyst has a negative optical effect at high radiation intensity leading to smaller degradation rates. This behavior is illustrated in Figure 8.

These conclusions, however, have to be considered in the proper context, given that in many cases the optimal catalyst concentration is determined

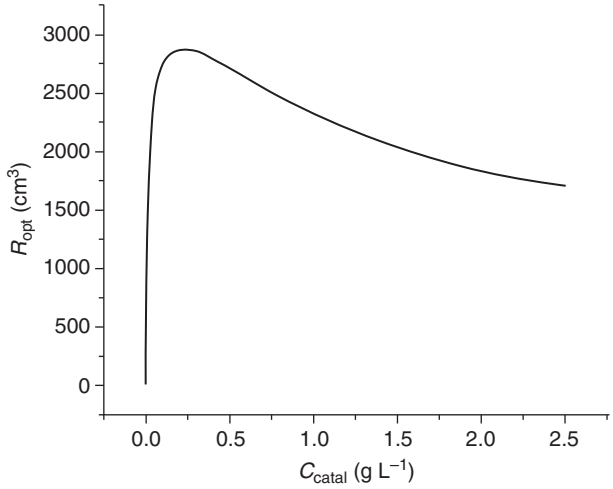

Figure 8 Reaction rate optical factor as a function of catalyst concentration for a parabolic trough solar photocatalytic reactor. Adapted from Arancibia-Bulnes and Cuevas 2004, with permission from Elsevier.

not by the optimal value of the RROF but by the requirement of having enough sites available for pollutant adsorption. Therefore, concentrations are often much higher than optimal from the optical point of view.

2.4. Solar photoreactors comparisons

Comparison of the performance between different photocatalytic reactors is not an easy task due to the diversity of experimental conditions and variables considered in each case. Work has been carried out by evaluating the reactor performance for the degradation of different model pollutants (Bahnemann et al., 1991; Bockelmann et al., 1995; Curcó et al., 1996a; Giménez et al., 1999; Goslich et al., 1997; Malato et al., 1997). The emphasis has been, however, on ranking concentrating versus nonconcentrating solar reactors. For instance, Bockelmann et al. (1995) carried out evaluation study of the degradation of dichloroacetic acid, as well as samples of wastewaters, with a parabolic trough (concentrating) and a thin film fixed bed reactor (1 sun). They observed that both concentrating and nonconcentrating collectors had inherent advantages and disadvantages, and it was not possible to decide unequivocally which system performed better.

More recently, reactors based on nonimaging collectors, like the CPC, have attracted interest (Blanco et al., 1999). These reactors share some of the advantages of both parabolic troughs and nonconcentrating reactors

(Malato et al., 1997) as mentioned previously. These features were confirmed in several studies using CPC and other nonconcentrating reactors as well as parabolic troughs (Curcó et al., 1996b; Giménez et al., 1999; Malato et al., 1997).

When comparing different solar collectors it is important to take into account the different quantities of radiation collected in each case. For a given receiver, the radiative power collected increases with aperture size (i.e., with concentration). However, this is not a linear effect and, for instance, a CPC with a two suns concentration ratio provides twice the aperture area of a nonconcentrating CPC. Nevertheless the power received by the tubular absorber is not doubled, because the former CPC misses around half of the diffuse radiation. Other important consideration is the fact that concentrating reactors are faster simply because they collect more radiation, which is associated with larger collector area.

For all the above reasons, when comparing different collectors it is necessary to consider the pollutant degradation against collected energy and not against irradiation time (Curcó et al., 1996b). One possibility for this assessment is to use the accumulated available energy, defined as the time integral of the UV power impinging on the collector's aperture area, per unit volume of the reactor

$$E_{\text{available}} = \int G_{\text{UV,global}}(t)\frac{A_{\text{a}}}{V_{\text{T}}}\,\mathrm{d}t \tag{17}$$

where $E_{\text{available}}$ is the accumulated available energy ($\mathrm{W\,m^{-3}}$), A_{a} is the collector's aperture area, V_{T} treated volume, and $G_{\text{UV,global}}(t)$ is the global UV irradiance ($\mathrm{W\,m^{-2}}$) at time t. This latter quantity is the radiative flux impinging on the collector surface due to both beam and diffuse solar rays, as measured for instance with a global UV radiometer. When working with experimental data the integral of Equation (17) has to be approximated as a sum over discrete radiation measurements taken on a prescribed sampling interval.

It is important to note that the accumulated available energy does not take into account the actual energy collected by each reactor. In fact, the actual collected energy is a function of concentration ratio, as concentrating collectors are able to capture only a $1/C_{\text{R}}$ fraction of the diffuse radiation. In order to reflect this, another quantity can be defined called the accumulated collected energy

where

$$E_{\text{collect}} = \int G_{\text{UV,collect}}(t)\frac{A_{\text{a}}}{V_{\text{T}}}\,\mathrm{d}t \tag{18}$$

$$G_{\text{UV,collect}} = (G_{\text{UV,global}} - G_{\text{UV,diffuse}}) + \frac{1}{C_{\text{R}}}G_{\text{UV,diffuse}} \tag{19}$$

Here $G_{UV,diffuse}(t)$ is the diffuse UV irradiance ($W\,m^{-2}$) at time t. The first term of the right-hand side of Equation (19) accounts for the contribution of beam solar rays (hence, global minus diffuse irradiance), and the second one for the diffuse solar rays captured by the system.

Bandala et al. (2004) and Bandala and Estrada (2007) carried out comparisons, for the degradation of oxalic acid and carbaryl, between tubular solar photocatalytic reactors with different mirror types: V-trough collector (VTC), CPC, PTC, and directly illuminated tubes (TC) (see Figure 9). All of the collectors tested were coupled to the same azimuthal solar tracking system to ensure the same irradiation conditions over them. This comparison gave results relatively similar for both CPC and VTC, with important gains observed over the PTC and the TC (Figure 10). While the PTC was able

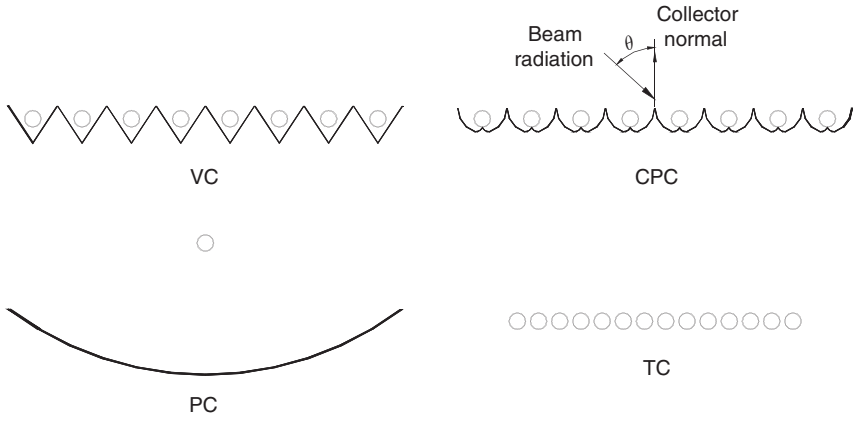

Figure 9 Different photoreactor geometries compared by Bandala et al. 2004, reprinted with permission from Elsevier.

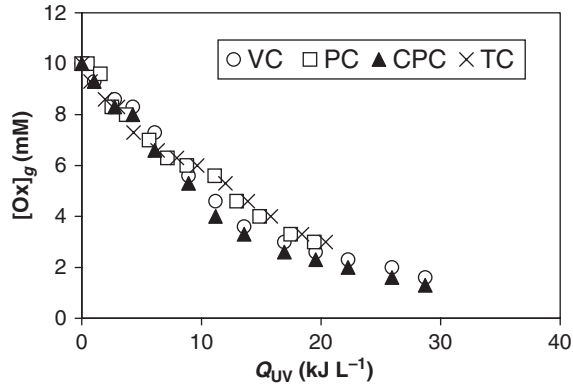

Figure 10 Photocatalytic degradation of oxalic acid in four different solar reactors as a function of accumulated energy (reprinted from Bandala et al., 2004, with permission from Elsevier).

to use less of the available solar UV radiation (only the beam part), it had a high optical efficiency. The same happened for TC, where the absence of a reflector reduces reflection losses. Nevertheless, it appears that the ability of the VTC and the CPC to distribute the radiation more homogeneously in the reactor walls is an important consideration and produces better results in the pollutant photodegradation process, with the CPC being ranked in the first place.

McLoughlin et al. (2004b) have also made a similar comparison between a VTC, a PTC, and a CPC for disinfection of water heavily contaminated with *Escherichia coli*, both by photocatalysis and by UV irradiation without catalyst. In this case the collectors did not track the sun but were inclined at local latitude with reactor tubes running east-west. It was also found that the CPC had the best performance, followed by the PTC and the VTC, which showed comparable results. It is necessary to point out that the PTC studied was of the nonconcentrating type with a very different configuration with respect to the one used by Bandala et al. (2004).

2.5. Concentrating CPC reactors

Photocatalysis is a rather inefficient process at moderate and high solar concentrations. This is due to the square root dependence of the photoconversion rate with radiation intensity (see Section 2.3). However, at low concentrations up to five suns, no such dependence has been observed (Román Rodríguez, 2001), because saturation conditions of the electron–hole generation in the catalyst are not reached. Actually, information about photocatalysis with low concentration solar reactors is scarce. This type of reactors has not been considered in the past probably because they do not make use of diffuse radiation. Jiménez and Salgado (2009) have studied the use of concentrating CPC photocatalytic reactors, with different concentration ratios between 1 and 2 suns. Four different CPC reactors with tubular receivers of the same size and having 1, 1.5, 1.75, and 2 suns concentrations were compared. Degradation of carbaryl, a pesticide widely used in Latin America, was studied. The catalyst was deposited by the sol–gel technique in long glass tubes that were fixed inside the reaction space (Figure 11).

The deposit was carried out in Duran glass tubes of 70 cm length and 0.6 cm outer diameter. The sol–gel technique (Brinker and Scherer, 1990) allows immobilizing the TiO_2 catalyst in the form of thin films over metallic and ceramic substrates, in particular glass. This deposition technique has the flexibility to permit modification of properties like particle size, surface area, crystalline structure, surface texture, photosensitivity, and chemical reactivity by controlling the process parameters, like the used reactives, solvent, drying temperature, and doping with different metal traces (see Gelover et al., 2004, and references therein). In the case considered, the films

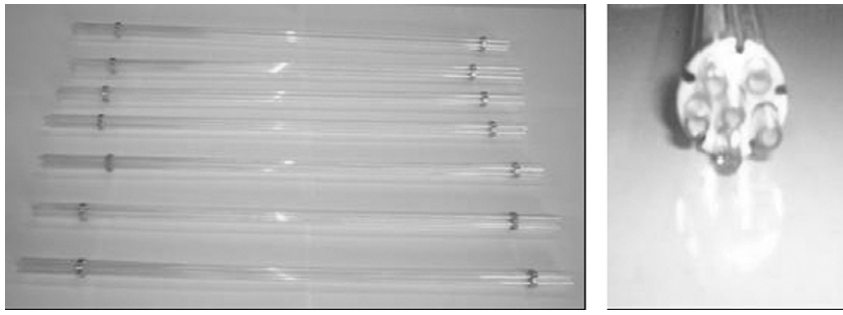

Figure 11 Glass tubes coated with sol-gel TiO_2 as support for catalyst to be used inside CPC reactors.

were 80 nm thick and had anatase crystalline structure (Gelover et al., 2004; Jiménez González and Gelover Santiago, 2007), with 15 nm average particle size.

Figure 12 presents the cross section of the four constructed CPCs. The collectors were mounted in parallel on a single structure to facilitate the comparison. This structure was oriented facing south with inclination equal to the local latitude (19°) and tubes oriented east-west (Figure 13). Each reactor processed 3 L of water in the recirculation batch mode.

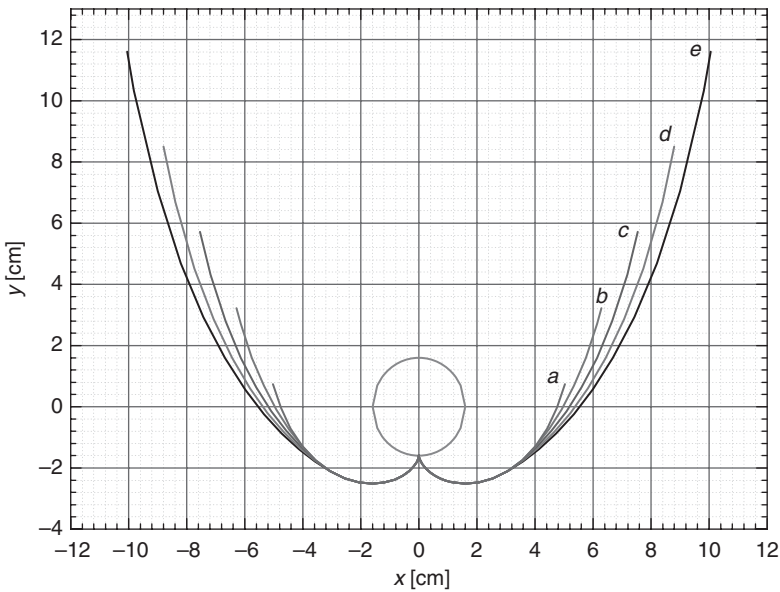

Figure 12 Cross section of the four CPC with 1, 1.5, 1.75, and 2 suns concentration.

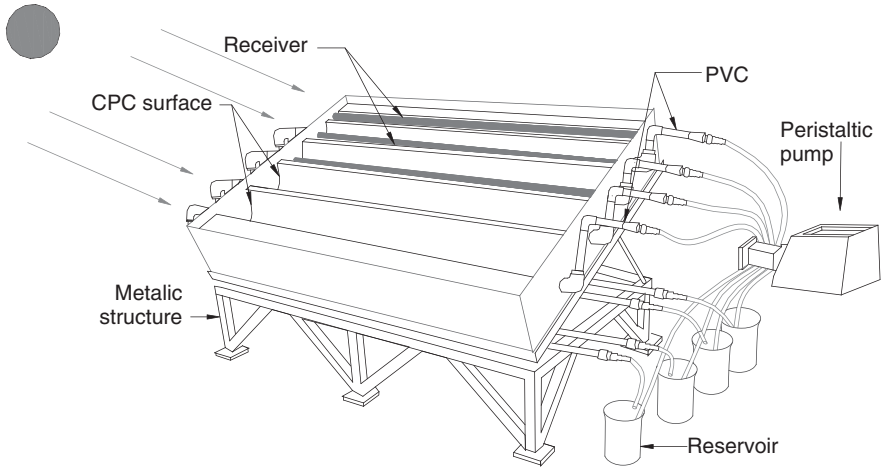

Figure 13 Multiple CPC test bed and experimental scheme. Each reactor tube contains five small glass tubes inside, supporting the TiO_2 catalyst.

As it has been discussed previously, for the 2 suns CPC the collected UV radiation is about 75% of the available solar radiation, while a nonconcentrating CPC captures in principle all the available radiation. However, as the aperture area of the 2 suns CPC is twice the aperture of the one sun system, the net result is that it collects 1.5 more energy. In the same way, the 1.5 and 1.75 suns reactors are able to capture 1.4 and 1.25 times more energy than the 1 sun system, respectively. The effect of these differences in the energy accepted by each system can be clearly seen in the degradation of carbaryl (Figure 14), where degradation proceeds faster as the concentration ratio increases.

When results are analyzed as a function of accumulated collected radiation (Equation (19)), as shown in Figure 15, it is found that the four collectors described utilize the captured energy with similar efficiency. This seems reasonable, considering that the four collectors have very similar designs, with concentration ratios being the only difference. It is also apparent that none of the collectors operates under a regime where catalyst electron–hole generation is saturated. Nevertheless, it seems as if the 2 suns collector performs slightly better than the others, at least at the beginning of the reaction period.

The four reactors were also compared on the basis of cost. Taking into account the cost of the aluminum reflectors it is found that the increase in the total cost of the 2 suns against the 1 sun collector is only of 15%. This is more than compensated by the fact that the same quantity of supported catalyst is used in both systems, so the overall cost per unit collector area is reduced.

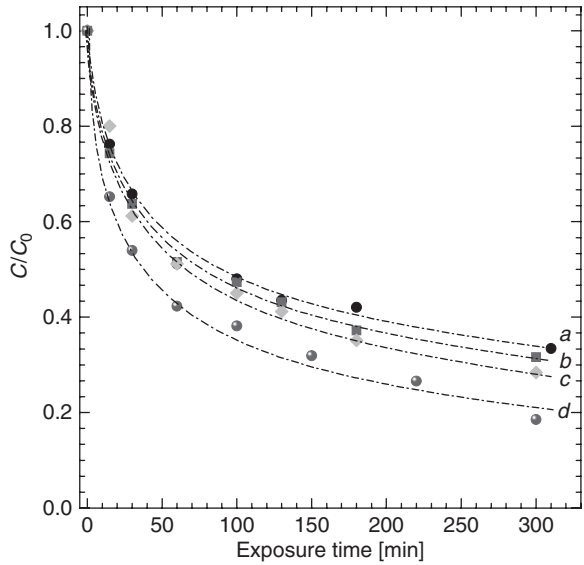

Figure 14 Evolution of carbaryl concentration as a function of time in four CPC reactors with 1 (*a*), 1.5 (*b*), 1.75 (*c*), and 2 (*d*) suns concentration ratio, respectively.

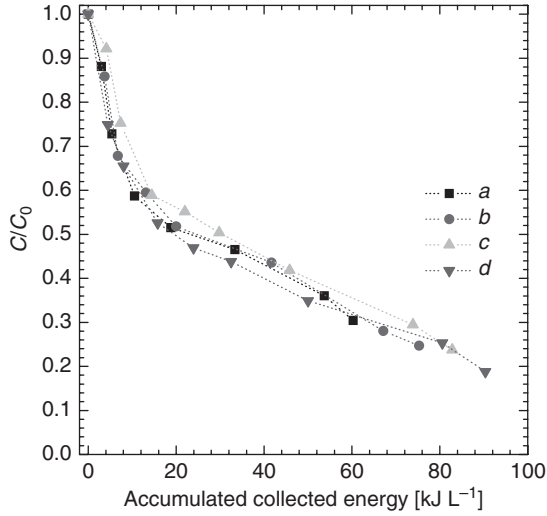

Figure 15 Evolution of carbaryl concentration as a function accumulated collected energy in four CPC reactors with 1 (*a*), 1.5 (*b*), 1.75 (*c*), and 2 (*d*) suns concentration ratio, respectively.

In addition to the above, the reduction in treatment time with concentration is also an attractive feature of the 2 suns collector, in spite of the fact that it misses around 25% of the available radiation. Due to the abundance of solar irradiation in the test site (Temixco, Morelos, Mexico), it does not appear that sacrificing a part of the UV radiation is such a great concern. However, in depth techno-economic analyses are required to support this assertion.

3. RADIATION TRANSFER IN PHOTOCATALYTIC REACTORS

As discussed previously, the radiative quantity of interest in photocatalysis is the local spectral power absorbed by the catalyst per unit volume $Q^{m}_{\text{abs-cat},\lambda}(\mathbf{r})$ ($\mathrm{W\,m^{-3}}$). This parameter is directly related to the number of photons available, per unit volume, and wavelength to carry out the excitation of electron–hole pairs.

Slurry photocatalytic reactors are characterized by the presence of catalyst particles with sizes in the micrometer and submicrometer range. Such small particles produce in general a fair amount of radiation scattering, as will be discussed later. Radiative transfer theory (Mahan, 2002; Modest, 2003) provides the tools to analyze and evaluate the absorption of radiation inside a scattering/absorbing medium.

Radiative transfer models can be very complicated and their solution cumbersome, so it is always desirable to have simplified tools for this analysis. Very simple and intuitive models can be developed in some cases to study radiation transfer inside photocatalytic reactors. However, it must be pointed out that these models must be well grounded in radiative transfer theory, in order to provide results that are consistent and of lasting engineering interest. Here, we present the basic concepts and discuss some approximations and methods that have been used.

3.1. Optical properties of the medium

Optical coefficients of the water/catalyst suspension are needed for carrying out radiative transfer calculations. When a beam of light propagates in a participating medium it can suffer absorption and scattering. Both processes reduce the intensity of this beam; in particular, scattering removes radiation from the beam and delivers it to beams propagating in other directions. The attenuation follows a Lambert–Beer type law, where the diminution of the intensity in a differential distance is proportional to intensity itself and to the distance traveled. The proportionality constant is the extinction coefficient of the medium β_λ ($\mathrm{cm^{-1}}$), which is the sum of the scattering σ_λ ($\mathrm{cm^{-1}}$) and absorption κ_λ ($\mathrm{cm^{-1}}$) coefficients.

$$\beta_\lambda = \kappa_\lambda + \sigma_\lambda \tag{20}$$

The extinction, absorption, and scattering coefficients depend on catalyst particle concentration C_p. If concentration is not extremely high, this dependence is linear

$$\beta_\lambda = C_{\text{catal}}\beta^*_{\lambda,\text{catal}}, \quad \kappa_\lambda = C_{\text{catal}}\kappa^*_{\lambda,\text{catal}}, \quad \sigma_\lambda = C_{\text{catal}}\sigma^*_{\lambda,\text{catal}} \tag{21}$$

where $\beta^*_{\lambda,\text{catal}}$, $\kappa^*_{\lambda,\text{catal}}$, and $\sigma^*_{\lambda,\text{catal}}$ are specific coefficients, independent of concentration. When radiation impinges with a particle, either absorption or scattering must occur. The fraction of radiation that is scattered is given by the quantity known as scattering albedo

$$\omega_\lambda = \frac{\sigma_\lambda}{\beta_\lambda} \tag{22}$$

The directional distribution of scattering is given by the phase function $\Phi_\lambda(\hat{\mathbf{s}} \cdot \hat{\mathbf{s}}')$. This function depends on the angle between the incident $\hat{\mathbf{s}}$ and scattered directions $\hat{\mathbf{s}}'$, $\cos \quad \theta_s = \hat{\mathbf{s}} \cdot \hat{\mathbf{s}}'$. The determination of the phase function requires elaborate experiments. It is common to use approximate phase functions, like the Henyey–Greenstein phase function $\Phi_{\text{HG},\lambda}$ (see, for instance, Modest, 2003), which can be used to approximate the real phase function for many types of particles

$$\Phi_{\text{HG},\lambda}(\hat{\mathbf{s}} \cdot \hat{\mathbf{s}}') = \frac{1 - g_\lambda^2}{[1 + g_\lambda^2 - 2g_\lambda \cos(\hat{\mathbf{s}} \cdot \hat{\mathbf{s}}')]^{3/2}} \tag{23}$$

Here g_λ is the wavelength-dependent asymmetry parameter (see Equation (36) below).

Several authors have addressed the determination of the optical properties of aqueous titanium dioxide suspensions in the context of photoreactor modeling (Brandi et al., 1999; Cabrera et al., 1996; Curcó et al., 2002; Salaices et al., 2001, 2002; Satuf et al., 2005; Yokota et al., 1999). Among the determined properties are extinction, scattering, and absorption coefficients, as well as the asymmetry parameter of the scattering phase function. In general the procedures involve fitting of a radiative transfer model to the experimental results for reflectance and transmittance of radiation.

In particular, Cabrera et al. (1996), Brandi et al. (1999), and Satuf et al. (2005) have determined optical parameters for TiO_2 particles of several commercial brands. The determinations were carried out by means of spectrophotometry experiments involving the measurement of specular reflectance and beam transmittance, as well as hemispherical transmittance and reflectance, of catalyst suspensions (Cabrera et al., 1996). By radiative transfer calculations with the discrete ordinates method (DOM), the values of the extinction and absorption coefficient and of the asymmetry parameter that better fitted the results of measurements were found. Actually, the extinction coefficients of Satuf et al. (2005) are the same as those of Brandi

et al. (1999), but the absorption coefficients are very different. The reason for this is the use of a different phase function in each case: Brandi et al. (1999) assumed an isotropic phase function for simplicity while Satuf et al. (2005) refined this previous work by taking into account the possibility of anisotropic scattering by means of the Henyey–Greenstein phase function.

3.2. Modeling dye degradation

When the photocatalytic degradation of a dye or of any other nontransparent contaminant is considered, the effect of the dye on the optical properties of the aqueous medium has to be accounted for. The dye absorbs radiation but does not scatter it; therefore, the scattering coefficient for the medium is equal to the scattering coefficient of the catalyst particles

$$\sigma_\lambda = C_{\text{catal}}\sigma^*_{\lambda,\text{catal}} \tag{24}$$

Here $\sigma^*_{\lambda,\text{catal}}$ ($\text{cm}^2\ \text{g}^{-1}$) is the specific scattering coefficient of the catalyst, which is independent of catalyst concentration.

On the other hand, at each wavelength, the absorption coefficient of the medium is a sum of the absorption coefficients of the dye and the catalyst

$$\kappa_\lambda = C_{\text{dye}}\kappa^*_{\lambda,\text{dye}} + C_{\text{catal}}\kappa^*_{\lambda,\text{catal}} \tag{25}$$

The specific absorption coefficient of the dye $\kappa^*_{\lambda,\text{dye}}$ ($\text{cm}^{-1}\,\text{ppm}^{-1}$) is the easiest to determine of all the optical parameters in this kind of problems. For dye concentrations which are not too high, one can expect that Lambert–Beer law is satisfied; that is, the transmittance of an aqueous solution of the dye should follow an exponential decay with concentration. This means that a linear relationship exists between the absorbance of the samples and dye concentration for each measured wavelength. Spectral measurements of the transmittance of solutions of the dye (in the absence of catalyst) for different concentrations can be made on a spectrophotometer. The specific absorption coefficient for different wavelengths is the slope of a straight line fit to these data, divided by the length of the spectrophotometer test cell.

For the optical properties of the catalyst the situation is somewhat more complicated. These optical properties have been determined for suspension of TiO_2 in water; that is, for catalyst particles surrounded by a nonabsorbing medium. In the present case the particles are surrounded by the absorbing aqueous dye solution and there is a possibility that their effective optical properties may be modified by this fact.

There has been some conceptual disagreement in the definition and interpretation of optical cross sections of small particles when the surrounding medium absorbs radiation (Bohren and Gilra, 1979; Lebedev et al., 1999; Mundy et al. 1974). Recently, an operational point of view has been adopted, which allows to carry out calculations for composite

media consisting of small particles embedded in absorbing hosts (Lebedev et al. 1999; Sudiarta and Chylek, 2001). In the case of commercial TiO_2 particles it is difficult to apply scattering theories to determine the optical properties of the catalyst particles due to lack of precise information about their microstructure. Nevertheless, some conclusions can be drawn from examination of the results reported in the literature: as is found in the cases studied by Mundy et al. (1974), Sudiarta and Chylek (2001), and Bruscaglioni et al. (1993) to observe appreciable effects in the extinction and scattering coefficients of the particles due to the presence of the dye, the imaginary part of the refractive index of the surrounding medium n_{imag} should be at least of the order 10^{-3}. This is not a definitive rule, but one based on the limited information available in the literature. The imaginary part of the index of refraction of the aqueous dye solution is related to the specific absorption coefficient by

$$n_{\text{imag}} = \frac{\kappa^*_{\lambda,\text{dye}}\, C_{\text{dye}}\, \lambda}{4\pi} \tag{26}$$

For instance, at $\lambda = 355\,\text{nm}$, for a concentration $C_{\text{dye}} = 120\,\text{ppm}$ of Acid Orange 24, it was obtained that $n_{\text{imag}} = 3.27 \times 10^{-7}$ (Villafán-Vidales et al., 2007). In that case it was concluded that it was not very likely that there was an important effect of the absorption of the dissolved dye in the optical properties of catalyst particles. However, this is not necessarily so in a general case, where results depend very much on the absorption coefficient of the dye and its concentration. Moreover, special experiments would have to be devised to measure the optical coefficients of TiO_2 suspended in strongly colored water.

In the simulation of the evolution of the dye concentration the radiative and kinetic problems cannot be decoupled, as was the case for nonabsorbing contaminants. Therefore, some kind of numerical procedure based on time discretization has to be applied for the solution of Equation (10). One possibility is to apply an Euler-type method that consists in the following steps (Villafán-Vidales et al., 2007):

1. Starting off from the initial dye (variable) and catalyst (constant) concentrations the absorption and scattering coefficients for these concentrations are evaluated. Then, these coefficients are used in a radiative transfer model to obtain e_{L} for a large number of points within the reactor volume.
2. Once the distribution of e_{L} has been evaluated, the integral of Equation (10) is calculated numerically over the illuminated part of the reactor, and from this equation the instantaneous degradation rate is obtained. Multiplying this rate by the time step of the method, which must be small compared to the total time required for the degradation process, one gets the decrease in dye concentration. That means that concentration

at step $(n+1)$ is obtained from the concentration at step (n) by an equation of the type

$$C_{\text{dye}}^{(n+1)} = C_{\text{dye}}^{(n)} + \left(\frac{\mathrm{d}C_{\text{dye}}}{\mathrm{d}t}\right)^{(n)} \Delta t \tag{27}$$

3. Once this new dye concentration is obtained, the process is repeated from step (1). This process is carried out for different TiO_2 concentrations.

3.3. The radiation transfer equation

The quantity that fully characterizes radiation in a medium is the spectral radiative intensity $I_\lambda(\mathbf{r}, \hat{\mathbf{s}})$ ($\mathrm{W\,m^{-2}\,\mu m^{-1}\,sr^{-1}}$). This quantity is the formalization of the intuitive concept of a ray of light. It characterizes the local amount of power traveling along a given direction, per unit wavelength, per unit area normal to this direction, and per unit solid angle. It depends on five variables: three spatial variables for the position vector $\mathbf{r}$ and two angular variables for the direction unit vector $\hat{\mathbf{s}}$.

The local spectral power absorbed by the catalyst can be expressed in terms of intensity and of the absorption coefficient of the catalyst by the following equation:

$$Q_{\text{abs-cat},\lambda}^{m} = \kappa_{\text{catal},\lambda} G_\lambda(\mathbf{r}) \tag{28}$$

where $G_\lambda(\mathbf{r})$ is called the local incident radiation, which is the total intensity impinging on a point from all directions

$$G_\lambda(\mathbf{r}) = \int_{4\pi} I_\lambda(\mathbf{r}, \hat{\mathbf{s}}')\mathrm{d}\Omega' \tag{29}$$

Another quantity of interest in the discussions to follow is the radiative flux vector $\mathbf{q}_\lambda(\mathbf{r})$ ($\mathrm{W\,m^{-2}\,sr^{-1}}$), which gives the net spectral flux of radiation along the preferential propagation direction in a given point. It is, in simple terms, intensity summed as a vector over all propagation directions

$$\mathbf{q}_\lambda(\mathbf{r}) = \int_{4\pi} \hat{\mathbf{s}}' I_\lambda(\mathbf{r}, \hat{\mathbf{s}}')\mathrm{d}\Omega' \tag{30}$$

The distribution of intensity of radiation in a scattering/absorbing medium can be obtained by solving the RTE (Mahan, 2002; Modest, 2003).

$$\frac{\mathrm{d}I_\lambda(\mathbf{r}, \hat{\mathbf{s}})}{\mathrm{d}s} = -\beta_\lambda I_\lambda(\mathbf{r}, \hat{\mathbf{s}}) + \frac{\sigma_\lambda}{4\pi} \int_{4\pi} I_\lambda(\mathbf{r}, \hat{\mathbf{s}}')\ \Phi_\lambda(\hat{\mathbf{s}} \cdot \hat{\mathbf{s}}')\mathrm{d}\Omega' \tag{31}$$

This equation gives the variation of the intensity of radiation, passing through point $\mathbf{r}$ in the medium, along the propagation direction $\hat{\mathbf{s}}$, when it travels a distance ds in that direction. Actually, this can be visualized not as a single equation but as an infinite set of coupled equations, one for each possible propagation direction. As expressed by the first term in the right-hand side of this equation, intensity is diminished due to both scattering and absorption (recall Equation (20)). The second term takes multiple scattering into account and couples all different propagation directions; that is, scattering takes some energy out from propagation direction $\hat{\mathbf{s}}'$ and redirects it into the direction under consideration $\hat{\mathbf{s}}$.

Basically, Equation (31) is a generalization of Lambert–Beer law to include multiple scattering effects; that is, the possibility not only that the intensity of a light beam entering a medium is decreased due to scattering, but also the possibility that some of this radiation may return eventually to the original propagation direction after several scattering events. In the case when the medium does not scatter (as is the case, for instance, in the photo-Fenton processes), this reduces to the ordinary Lambert–Beer law of propagation

$$\frac{\mathrm{d}I_\lambda(\mathbf{r},\hat{\mathbf{s}})}{\mathrm{d}s} = -\kappa_\lambda\, I_\lambda(\mathbf{r},\hat{\mathbf{s}}) \tag{32}$$

3.4. Methods of solution of the RTE

Due to the integro-differential nature of the RTE, it is a complex equation and analytical solutions are not available, except for the simplest problems. Several methods have been devised to overcome this limitation, either numerical solutions of the exact RTE or simplified models that do have analytical solutions. It is also possible that we need to solve numerically such a simplified model, in which case the advantages of the simplification must be carefully considered against the greater exactness of solving the RTE numerically.

Among the numerical models to solve the exact RTE we can mention the DOM (Modest, 2003) and the Monte Carlo method (MCM) (Mahan, 2002). The greatest complication in solving the RTE is how to deal with the integral term in the right-hand side of the equation. The DOM discretizes the infinite number of directions involved in Equation (31) to a finite number of directions $\hat{\mathbf{s}}_i$, optimally chosen according to the geometry of the problem. In such a way, the integral term is reduced to a sum over the chosen propagation directions. The problem then consists in the solution of a coupled system of linear differential equations, one for each propagation direction, at every point inside the reactor volume. The differential term in the left-hand side must also be discretized, for which the left-hand side of

the RTE is rewritten in an equivalent form where differentiation is more explicitly expressed

$$\hat{\mathbf{s}} \cdot \nabla I_\lambda(\mathbf{r}, \hat{\mathbf{s}}) = -\beta_\lambda I_\lambda(\mathbf{r}, \hat{\mathbf{s}}) + \frac{\sigma_\lambda}{4\pi} \int_{4\pi} I_\lambda(\mathbf{r}, \hat{\mathbf{s}}') \ \Phi_\lambda(\hat{\mathbf{s}} \cdot \hat{\mathbf{s}}') \mathrm{d}\Omega' \tag{33}$$

The present description of the method is somewhat oversimplified, because boundary conditions, directions, and spatial discretization must be carefully established in every case for the geometry at hand.

The DOM has been extensively and successfully applied to photocatalytic reactors by the Santa Fe (Argentina) group (see Cassano and Alfano 2000, and references therein) and verified against experimental results (Brandi et al., 1999; Romero et al., 2003). Also Trujillo et al. (2007) have recently used a variant of the DOM, called finite volume scheme to model the effect of air bubbles injected in a fixed catalyst reactor.

The MCM consist in tracking numerically the propagation of a large sample of individual photons inside the system and evaluating the desired parameters as statistical averages over these samples (Mahan, 2002). Each step in the propagation is considered as a random event and simulated by generating random numbers according to prescribed probability distributions (Arancibia-Bulnes and Ruiz-Suárez, 1999; Yokota et. al., 1999).

For instance, at a wall or at an interface between two media (as may be the water surface), the reflectance and transmittance are interpreted as probabilities of reflection and transmission, respectively. The outcome of the interaction of a photon with the wall is decided by generating a random number uniformly distributed between zero and one, and comparing this number with the respective wall reflectance. The propagation distance before colliding with a catalyst particle follows an exponential probability distribution with β_λ^{-1} as the attenuation coefficient. Then, to simulate propagation a random number is generated according to this distribution to decide where the next collision will happen. At a collision, the scattering albedo ω_λ is interpreted as the probability of scattering and $(1-\omega_\lambda)$ as the probability of absorption. When a photon is absorbed, its history is terminated, but when it is scattered a new propagation direction must be chosen and the process continued. The phase function is interpreted then as a probability distribution for scattering angles.

The MCM has been used to simulate tubular solar photocatalytic reactors, like parabolic troughs (Arancibia-Bulnes et al., 2002a), CPC (Arancibia-Bulnes et al., 2002b), and also of flat plate geometry (Cuevas et al., 2004). Also it has been used to simulate flat lamp reactors (Brucato et al., 2006) or to obtain optical coefficients by comparison with transmission results from an experimental cell (Yokota et al., 1999).

Among the approximate analytical models there are the many-flux models. These models are similar to the DOM, in the sense that the integral term

of the RTE is approximated as a sum by taking into account only a limited number of propagation directions. The simplest of these are two flux models, like the classical Schuster–Schwarzchild and Kubelka–Munk (Ishimaru, 1997) models, which are applicable to plane parallel media where transversal directions are much larger than propagation depth. Actually these are the simplest possible models able to take multiple scattering into account. In these models only the forward and backward propagation directions are considered, which correspond to two diffuse radiation fluxes, propagating to the inside and to the outside of the medium, respectively. Two flux models have been used by Brucato and Rizzuti (1997) and Brucato et al. (2006)

Other authors have also used approximate methods to solve the radiation problem. Li Puma and Yue (2003) used a thin film slurry model which does not include scattering effects. More recently, Li Puma et al. (2004), Brucato et al. (2006), and Li Puma and Brucato (2007) have used six flux models for different geometries. Salaices et al. (2001, 2002) used a model which allows for an adequate evaluation of the absorbed radiation in terms of macroscopic balances, based on radiometric measurements. They measured separately total transmitted radiation and nonscattered transmitted radiation, modeling the decay of both radiative fluxes with concentration by exponential functions.

Of a different nature is the P1 approximation (Modest, 2003), also known as the diffusion approximation (Ishimaru, 1997). Here the number of propagation directions is not restricted, but instead it is assumed that energy distributes quite uniformly over all these directions, as will be described in the next section. This approximation is the lowest order of the spherical harmonics method (also known as the Pn approximation). It is more versatile than two- and four-flux models, because it lends itself more easily to different geometries.

4. THE P1 APPROXIMATION

The P1 approximation assumes that the angular distribution of radiation intensity is almost isotropic within the medium; that is, the radiative energy that reaches any given point inside the reactor comes almost equally from all possible directions. This requires a great deal of scattering, in order to erase from the radiation field the directional behavior originated from its sources. Nevertheless, the radiation intensity I_λ cannot be completely uniform for all directions $\hat{\mathbf{s}}$, because there would be no net energy propagation in any direction in such a case. Therefore, the P1 approximation assumes that radiation intensity is slightly higher in the direction of the net flux. Mathematically, intensity is expressed as a linear function of the components of the propagation vector $\hat{\mathbf{s}} = (s_x, s_y, s_z)$

$$I_\lambda(\mathbf{r}, \hat{\mathbf{s}}) = \frac{1}{4\pi}[G_\lambda(\mathbf{r}) + 3\mathbf{q}_\lambda(\mathbf{r}) \cdot \hat{\mathbf{s}}] \tag{34}$$

where the second term in the right-hand side should be much smaller than the first, and subsequent terms with higher order dependence on direction are neglected.

Inserting Equation (34) into the RTE, it is possible to carry out analytically the integral in the right-hand side of this equation. After some algebra (Modest, 2003, pp. 511–514) it is obtained that

$$\mathbf{q}_\lambda(\mathbf{r}) = -\left[3\beta_\lambda(1-g_\lambda\omega_\lambda)\right]^{-1}\nabla G_\lambda(\mathbf{r}) \tag{35}$$

where g_λ is known as asymmetry parameter and is given by

$$g_\lambda = \frac{1}{4\pi}\int_{4\pi}\Phi_\lambda(\hat{\mathbf{s}}\cdot\hat{\mathbf{s}}')\,(\hat{\mathbf{s}}\cdot\hat{\mathbf{s}}')\,\mathrm{d}\Omega' \tag{36}$$

This parameter describes the scattering directional behavior of the particles; for instance, it equals 1 for purely forward scattering, −1 for purely backwards scattering, and 0 for isotropic scattering.

A physical interpretation of Equation (35) is possible if one notes that it is mathematically analogous to Fourier law of heat conduction. The constant factor in the right-hand side plays the role of thermal conductivity, and the local incident radiation $G_\lambda(\mathbf{r})$ plays the role of temperature. In that sense, differences in the latter variable among neighboring regions in the medium drive the "diffusion" of radiation toward the less radiated zone. Note that the more positive the asymmetry parameter, the higher the "conductivity"; that is, forward scattering accelerates radiation diffusion while backscattering retards it.

Besides the approximate Equation (35), another more fundamental equation from radiative transfer theory also relates G_λ with $\mathbf{q}_\lambda$ (see, for instance, Modest, 2003, pp. 312–314)

$$\nabla\cdot\mathbf{q}_\lambda(\mathbf{r}) = -\kappa_\lambda G_\lambda(\mathbf{r}) \tag{37}$$

Taking the divergence of Equation (35) and substituting it into Equation (37), a second-order partial differential equation of the Helmholtz type is finally obtained for the P1 approximation

$$\nabla^2 G_\lambda = k_{\mathrm{d},\lambda}^2\, G_\lambda \tag{38}$$

where k_d is a wavelength-dependent constant (sometimes called diffusion constant) given by

$$k_{\mathrm{d},\lambda} = \sqrt{3(1-\omega_\lambda\, g_\lambda)\kappa_\lambda\beta_\lambda} \tag{39}$$

To continue the analogy with heat conduction, it can be seen that this equation is analogous with the steady-state equation of heat conduction in the presence of heat sources.

Note that, within the assumptions of the P1 approximation, solving Equation (38) is entirely equivalent to solving the RTE, because once G_λ is known, I_λ can be evaluated by using Equations (34) and (35).

To solve Equation (38) boundary conditions which describe the reflection and transmission of radiation at the boundaries are required. In principle, boundary conditions can only be established in a rigorous manner for the radiative intensity, not for G_λ, because the optical properties of the interfaces depend on the direction of incidence of radiation. Because the P1 approximation solves for an integrated quantity like G_λ instead, approximate boundary conditions must be established (Modest, 2003). One possibility is the Marshak boundary condition (Marshak, 1947), which comes from considering the continuity of the radiative flux through the interface. If this continuity is considered together with the assumption (34) of the P1 approximation and Equation (37), the following equation is obtained (Spott and Svaasand, 2000)

$$(1-2\rho_1)\,G_\lambda-(1+3\rho_2)\frac{2\hat{\mathbf{n}}\cdot\nabla G_\lambda}{3\beta_\lambda(1-\omega_\lambda g_\lambda)}=4q_{\mathrm{e},\lambda} \tag{40}$$

Here $q_{e,\lambda}$ accounts for any external flux coming through the surface, $\hat{\mathbf{n}}$ the surface normal, and ρ_i is the ith moment of the surface reflectance function $\rho(\hat{\mathbf{n}}\cdot\hat{\mathbf{s}})$ given by

$$\rho_i=\int_{2\pi}\rho(\hat{\mathbf{n}}\cdot\hat{\mathbf{s}}')\,(\hat{\mathbf{n}}\cdot\hat{\mathbf{s}}')^i\,\mathrm{d}\Omega' \tag{41}$$

4.1. General solution of the P1 approximation for solar tubular reactors

As discussed previously, several solar photoreactor geometries can be reduced to cylindrical glass tubes externally illuminated by different types of reflectors, like parabolic troughs, CPC, V-grooves, or without reflector, directly illuminated by the sun. In this section the general solution of the P1 approximation for this type of photoreactors is reported. This general solution is applicable to any particular reactor if the flux distribution impinging on the wall of the tubular reaction space is known.

To model the radiation field for a tubular reactor, Equation (38) is written in cylindrical coordinates. If the tube is slender we can neglect end effects and the radiative flux is independent of the longitudinal variable z, then

$$\frac{1}{r}\frac{\partial}{\partial r}\left(r\frac{\partial G_\lambda}{\partial r}\right)+\frac{1}{r^2}\frac{\partial^2 G_\lambda}{\partial\theta^2}=k_{\mathrm{d},\lambda}^2 G_\lambda \tag{42}$$

The general solution of this equation can be obtained by the standard method of separation of variables

$$G_\lambda(r,\ \theta) = \sum_{n=0}^{\infty} [A_n \cos(\delta_n \theta) + B_n \sin(\delta_n \theta)][C_n\ \mathrm{I}_n(k_{\mathrm{d},\lambda} r) + D_n\ \mathrm{K}_n(k_{\mathrm{d},\lambda} r)] \quad (43)$$

In this equation, I_n and K_n are nth order modified Bessel functions of the first and second kind (Olver, 1972), respectively. These functions behave somewhat like increasing and decreasing exponentials, respectively. The eigenvalues δ_n are obtained easily in this case by the consideration that physically local incident radiation must be periodical when the angle θ completes a full turn around the tube

$$G(r, 0) = G(r, 2\pi) \quad (44)$$

therefore

$$\delta_n = n \quad (45)$$

Another consideration that can be applied is observing that the K_n functions diverge at the center of the reactor ($r = 0$) and therefore cannot be present in the solution. Taking this into account, we obtain as general solution for any tubular solar reactor

$$G_\lambda(r,\ \theta) = \sum_{n=0}^{\infty} [E_n \cos(n\theta) + F_n \sin(n\theta)]\ I_n(k_{\mathrm{d},\lambda} r) \quad (46)$$

In terms of the angular variable, this expression is a Fourier series. To obtain the constants E_n and F_n that appear on this equation one must apply the boundary condition (40) at the tube wall ($r = r_0$), which in this case reduces to

$$(1 - 2\rho_1)\ G_\lambda(r_0) + (1 + 3\rho_2)\ \frac{2}{3\beta_\lambda(1 - \omega_\lambda g_\lambda)}\ \frac{\partial G_\lambda}{\partial r}\bigg|_{r=r_0} = 4 q_{\mathrm{e},\lambda} \quad (47)$$

For applying this condition, in turn it is necessary to expand the total solar radiative flux entering trough the tube wall (formed by the directly incident part plus that reflected by the mirrors) into a Fourier series

$$q_{\mathrm{e},\lambda}(\theta) = \sum_{n=0}^{\infty} [Q_n \cos(n\theta) + R_n \sin(n\theta)] \quad (48)$$

With this, the unknown coefficients are obtained.

$$E_n = 4 Q_n \left\{ (1 - 2\rho_1)\ \ I_n(k_{\mathrm{d},\lambda} r_0) + 2 k_{\mathrm{d},\lambda} \left[\frac{(1 + 3\rho_2)}{3\beta_\lambda(1 - \omega_\lambda g_\lambda)} \right] I_n'(k_{\mathrm{d},\lambda} r_0) \right\}^{-1} \quad (49)$$

$$F_n = 4R_n \left\{ (1-2\rho_1)\ \mathrm{I}_n(k_{\mathrm{d},\lambda} r_0) + 2k_{\mathrm{d},\lambda} \left[\frac{(1+3\rho_2)}{3\beta_\lambda(1-\omega_\lambda g_\lambda)} \right] I_n'(k_{\mathrm{d},\lambda} r_0) \right\}^{-1} \quad (50)$$

To use this general solution, it is only necessary to obtain the distribution of the radiative flux on the reactor wall, say by applying a ray tracing method to the solar collector, and to expand the resulting distribution of radiative flux in a Fourier expansion like (48). Then the solution inside the reactor is obtained.

Let us consider the particular case of a tube directly illuminated only by beam solar radiation. Graphically this looks like in Figure 16.

The radiative flux on the boundary can be expressed by the simple equation

$$q_{\mathrm{e},\lambda}(\theta) = \tau\, G_{\mathrm{UV,beam}} \cos(\theta) \quad (51)$$

where τ is the transmittance of the glass tube (assumed constant for simplicity), and $G_{\mathrm{UV,beam}}$ is the measured UV irradiance of solar beam radiation. In this case the coefficients of the Fourier expansion are all zero except by

$$Q_1 = \tau\, G_{\mathrm{UV,beam}} \quad (52)$$

A slightly different calculation must be done to take also into account the diffuse component of UV solar radiation in the solution.

4.2. Solution for a parabolic trough reactor

The analytical expression for the radiation flux distribution produced on the wall of a tubular receiver by a PTC (Figure 17) has been calculated by Jetter (1986, 1987). Jetter's method is applied here to a particular PTC collector that has been used in our research group to study the degradation of several

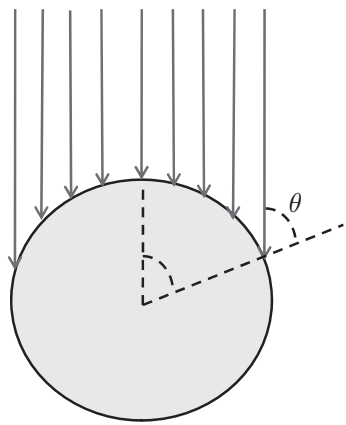

Figure 16 Tubular reactor illuminated by beam solar radiation.

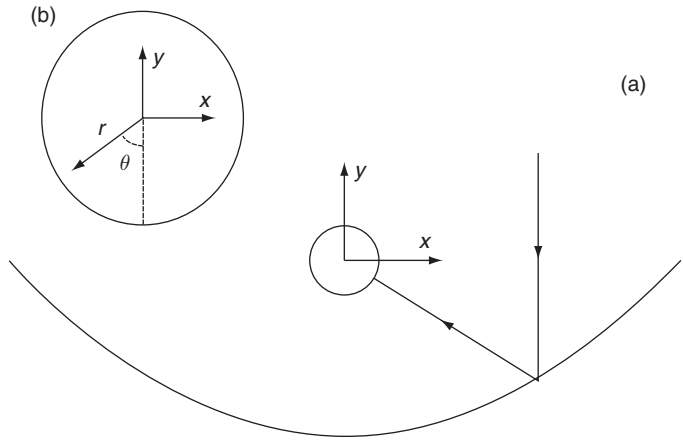

Figure 17 Geometry of the parabolic trough and reactor tube (a), and coordinate systems inside the tube (b) (reprinted from Arancibia-Bulnes and Cuevas, 2004, with permission from Elsevier).

pollutants (Arancibia-Bulnes et al., 2002a,b; Bandala et al., 2002; Gelover et al., 2000; Jiménez et al., 2000). The characteristics of this concentrator are tube diameter 2.45 cm, length 172 cm, concentrator lateral aperture 106 cm, focal length 27 cm, rim angle 90°, average UV reflectance of mirror 75%, and average UV transmittance of glass reactor 85%. The surface reflection error of the mirror has been determined as 7 mrad. The resulting distribution is presented in Figure 18. The distribution is presented as flux concentration, which is the flux distribution divided by the beam solar radiation incident in the collector.

Ten terms were needed in the Fourier series to approximate adequately the distribution in Figure 18 and to reach convergence in the solution for the local incident radiation (Arancibia-Bulnes and Cuevas, 2004). An example of the obtained distribution of volumetric absorbed power is presented in Figure 19, for the cross section of the reactor, at a wavelength of 325 nm, and considering a concentration of 0.15 g L^{-1} of Aldrich TiO_2 catalyst. The peaks observed on the graph correspond with the peaks of the entering flux of Figure 18.

4.3. Solution for an annular lamp reactor

Even though this chapter is devoted mostly to solar photocatalytic reactors, we would like to discuss the modeling of an annular lamp reactor, as a different example of the application of the P1 approximation. This problem was studied (Cuevas et al., 2007) with reference to a particular reactor known as photo CREC-water II (Salaices et al., 2001, 2002). Equation (38) is again written in cylindrical coordinates. Nevertheless in this case the

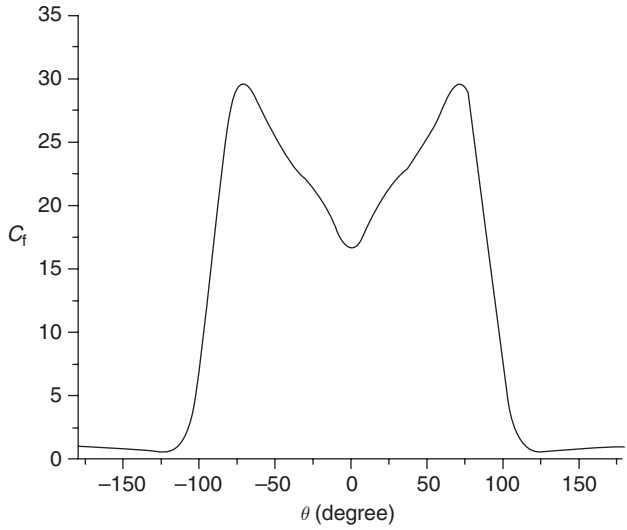

Figure 18 Flux concentration distribution of a 90° rim angle parabolic trough solar concentrator. Adapted from Arancibia-Bulnes and Cuevas (2004), with permission from Elsevier.

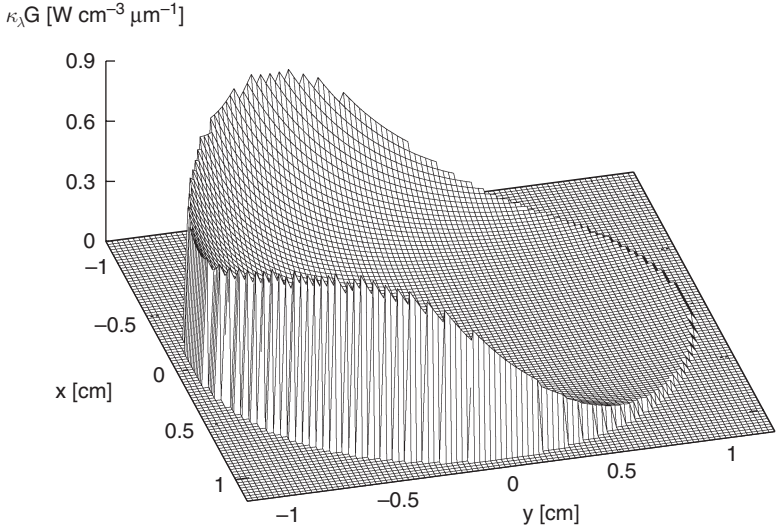

Figure 19 Distribution of spectral volumetric absorbed power inside a tubular reactor illuminated by a 90° rim angle parabolic trough solar concentrator. Wavelength 325 nm and catalyst concentration 0.15 g L^{-1} (Reprinted from Arancibia-Bulnes and Cuevas, 2004, with permission from Elsevier).

incident flux is the same for the whole reactor circumference, but it may depend on z if the flux from the lamp does so.

$$\frac{1}{r}\frac{\partial}{\partial r}\left(r\frac{\partial G_\lambda}{\partial r}\right)+\frac{\partial^2 G_\lambda}{\partial z^2}=k_{\mathrm{d},\lambda}^2 G_\lambda \tag{53}$$

The solution is symmetrical with respect to the center of the lamp ($z = L/2$) in the z coordinate due to the symmetry of the entering flux (Salaices et al., 2002). Therefore the problem is solved only in the range [0; $L/2$]. After applying suitable Marshak boundary conditions in the longitudinal variable to the general solution of this equation it is obtained that

$$G_\lambda(r,\ z)=\sum_{n=0}^{\infty} f_n(z)[E_n\ \mathrm{I}_0(x_n)+F_n\ \mathrm{K}_0(x_n)] \tag{54}$$

where

$$x_n=\sqrt{k_{\mathrm{d},\lambda}^2+\delta_n^2}\,r \tag{55}$$

The eigenfunctions f_n are given by

$$f_n(z)=\left[\cot\left(\frac{\delta_n L}{2}\right)\cos(\delta_n z)+\sin(\delta_n z)\right]C_n^{-1/2} \tag{56}$$

with

$$C_n=\frac{1}{2}\csc^2\left(\frac{\delta_n L}{2}\right)\left[1-\left(\frac{2}{\delta_n L}\right)\cos\left(\frac{\delta_n L}{2}\right)\sin\left(\frac{\delta_n L}{2}\right)\right] \tag{57}$$

And the eigenvalues δ_n must be obtained this time by the solution of the following transcendental equation

$$\cot\left(\frac{\delta_n L}{2}\right)=\left(\frac{\delta_n L}{2}\right)\frac{4(1+\rho_\mathrm{p})}{3(1-\rho_\mathrm{p})(1-g_\lambda\omega_\lambda)\beta_\lambda L} \tag{58}$$

Boundary conditions are also applied for the variable **r**, at the two cylindrical walls, from which explicit expressions are obtained for the constants in the solution. Figure 20 presents an example of a distribution of local incident radiation inside the reactor, as a function of the longitudinal and radial coordinates

The theoretical model developed here was compared (Cuevas et al., 2007) with measurements of radiative flux transmission through a series of observation windows in the photo CREC-Water II reactor (Salaices et al., 2001).

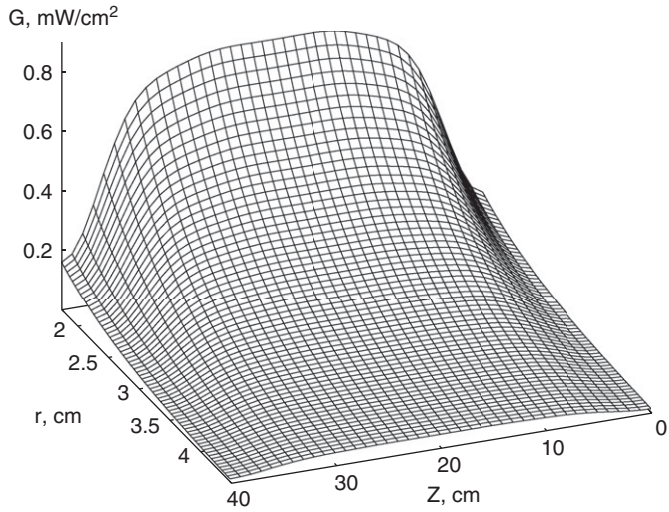

Figure 20 Distribution of the local incident radiation inside the reactor volume, for a catalyst concentration of 0.05 g L^{-1} (Adapted from Cuevas et al., 2007, with permission from Elsevier).

4.4. Applicability of the P1 approximation

The main limitation of the P1 approximation seems to be its applicability mainly to participating media with high optical depths (Cuevas et al., 2007). Optical depth is defined as

$$d_{\text{opt}} = \beta_{\lambda} D = (\beta^{*}_{\lambda,\text{catal}} C_{\text{catal}} + \beta^{*}_{\lambda,\text{dye}} C_{\text{dye}}) D \tag{59}$$

where D is a characteristic spatial distance that radiation crosses inside the participating medium (reaction space); for example, the tube radius in a parabolic trough, the depth of a flat plate photoreactor, or the radial distance between the concentric tubes in an annular photoreactor. Optical depth equals the number of photon mean free paths that this characteristic distance spans. A photon traversing the medium would experiment on the average at least a number of collisions equal to this optical depth before reaching a wall. So, high optical depths imply a great deal of scattering, which is the necessary requirement to have almost isotropic intensity distribution, as required by the P1 approximation.

It would appear that the above requirement imposes strong limitations to the use of the P1 approximation, but this is really not so; in practice, the prevailing situation is operation of the reactors at high optical depths, based on the characteristic dimensions of reacting spaces and the typical catalyst concentrations used (Cuevas et al., 2007). This seems contradictory at first, because from the point of view of radiative transfer the optimal catalyst

concentrations correspond to optical depths of order unity (Pasqualli et al., 1996). For smaller optical depths there is the risk that much of the radiation go out from the reactor without being absorbed, while for optical depths of order 10, radiation is absorbed almost immediately as it enters the reactor, leaving a large portion of the volume almost in the dark (Arancibia-Bulnes and Cuevas, 2004). In spite of this, much larger catalyst concentrations may be seen to give the maximum reaction rates, due to the need for more adsorption sites for the pollutants. A trade-off occurs: catalyst concentration should decrease in inverse proportion to the increase in the size of the reaction space, to maintain good illumination of the whole volume, while at the same time it should stay proportional to the pollutant concentration, to ensure availability of adsorption sites.

5. CONCLUSIONS AND PERSPECTIVES

This chapter reviews some of the main topics involved in the design and modeling of solar photocatalytic reactors, with particular emphasis on the authors' research experience. Solar photons are source of energy that initiates photocatalytic degradation. Thus, proper consideration of radiative processes is key to address this subject. The determination of the directional and spectral characteristics of solar UV radiation, the interaction of the catalyst with radiation inside reaction spaces, the optical design of solar collectors, and the optical properties of the materials involved are all subjects where these concepts are necessary. Therefore, developments in this area should be solidly grounded on the fields of solar collector optics and radiative transfer, besides the more traditional chemical engineering aspects involved. This requires a multidisciplinary approach.

Although different solar photoreactors have been developed in the last 20 years, each one with its own advantages and limitations, there is still room for new designs and innovative ideas. Nowadays, CPC appear as one of the most promising alternatives among solar photocatalytic reactors. The concepts of nonimaging optics, with its emphasis in efficient energy collection can also be a very useful in future developments.

The supporting of the TiO_2 in extended surfaces, glass beads, or other types of supports offers many possibilities for new designs and concepts. Modeling of radiative transfer in both slurry and fixed catalyst reactors is a necessary tool for the full understanding of the effect of the different design parameters in the performance of photoreactors. This should be accompanied with advances in material science, in order to develop improved catalysts that help reducing costs, making these processes economically viable.

ACKNOWLEDGMENTS

This work has been partially supported by CONACYT grants 56918, 49895-Y, UNAM grant 372311721 and PUNTA program. J. J. Quiñones Aguilar, R. Morán Elvira, M. L. Ramón García, I. Salgado, and F. Payán are acknowledged for technical support.

LIST OF SYMBOLS

A_a	aperture area of solar collector, m^2
A_n	constant
A_r	receiver area of solar collector, m^2
B_n	constant
c	speed of light in vacuum, $2.998 \times 10^8 m\,s^{-1}$
C_{catal}	catalyst concentration, $g\,L^{-1}$
C_{dye}	dye concentration, $g\,L^{-1}$
$C_{dye}^{(n)}$	dye concentration at time step n, $g\,L^{-1}$
C_n	normalization constant for the nth eigenfunction
C_n	constant
C_p	local pollutant concentration, mM
$C_{p,av}$	average pollutant concentration, mM
C_R	concentration ratio, suns
$C_{R,max}$	maximum solar concentration ratio of collector, suns
d_{opt}	optical depth
D	characteristic reactor spatial dimension, cm
e_L	local volumetric rate of photon absorption, $E\,m^{-3}\,s^{-1}$
$E_{available}$	accumulated available energy, $J\,m^{-3}$
$E_{collect}$	accumulated collected energy, $J\,m^{-3}$
E_n	constant
E_λ	photon energy, J
F_n	constant
f_n	normalized nth eigenfunction of an ordinary differential equation
F_1	function dependent on component concentration, $mM\,s^{-1}$
F_2	function depending on the LVREA
g_λ	asymmetry parameter
$G_{UV,global}$	global UV solar irradiance, $W\,m^{-2}$
$G_{UV,diffuse}$	diffuse UV solar irradiance, $W\,m^{-2}$
$G_{UV,beam}$	beam UV solar irradiance, $W\,m^{-2}$
$G_{UV,collect}$	collected UV solar irradiance, $W\,m^{-2}$
G_λ	local incident radiation, $W\,m^{-2}\,\mu m^{-1}$
h	Planck's constant, $6.626 \times 10^{-34}\,J\,s$
I_λ	radiation intensity, $W\,m^{-2}\,sr^{-1}\,\mu m^{-1}$
I_0, K_0	modified Bessel functions of order zero

I_n, K_n	modified Bessel functions of nth order
$k_{\mathrm{d},\lambda}$	radiation diffusion coefficient, cm^{-1}
$k_{\mathrm{O},i}$	kinetic parameter of the ith intermediate oxidation, $\mathrm{mM}^{-1}\,\mathrm{s}^{-1}$
k_{e}	electron–hole generation rate constant, s^{-1}
k_{E}	constant for electron capture by oxidant agent, s^{-1}
k_{F}	constant for hole capture by reducing agent, s^{-1}
k_{R}	electron–hole recombination rate constant, $\mathrm{mM}^{-1}\,\mathrm{s}^{-1}$
k_{α}	kinetic constant for pollutant oxidation, $\mathrm{mM}^{-1}\,\mathrm{s}^{-1}$
L	reactor tube length, cm
$\hat{\mathbf{n}}$	unit vector normal to a surface
n_{imag}	imaginary part of the index of refraction of the aqueous dye solution
N_{A}	Avogadro's number, $6.022 \times 10^{23}\,\mathrm{mol}^{-1}$
$Q^{m}_{\mathrm{abs-cat},\lambda}$	volumetric power absorbed by the catalyst, $\mathrm{W\,m}^{-2}\,\mu\mathrm{m}^{-1}$
Q_n	constant
$\mathbf{q}_{\lambda}$	radiative flux vector, $\mathrm{W\,m}^{-2}\,\mu\mathrm{m}^{-1}$
$q_{\mathrm{e},\lambda}$	external flux entering through the reactor wall, $\mathrm{W\,m}^{-2}\,\mu\mathrm{m}^{-1}$
$\mathbf{r}$	position vector, m
r	radial coordinate, m
r_0	radius of tubular receiver, m
$[R_i]$	concentration of the ith degradation intermediate, mM
R_n	constant
R_{opt}	reaction rate optical factor, cm^3
s	linear coordinate along propagation direction $\hat{\mathbf{s}}$, m
$\hat{\mathbf{s}}$	unit propagation direction vector
s_x, s_y, s_z	Cartesian components of direction vector
t	time, s
V_{T}	treated volume, m^3
V_{R}	illuminated (reactor) volume, m^3
x, y, z	Cartesian coordinates, m
x_n	scaled radial coordinate

Greek letters

β_{λ}	extinction coefficient of the medium, cm^{-1}
$\beta^{*}_{\lambda,\mathrm{catal}}$	specific absorption coefficient of the catalyst, $\mathrm{cm}^2\,\mathrm{g}^{-1}$
$\beta^{*}_{\lambda,\mathrm{dye}}$	specific absorption coefficient of the dye, $\mathrm{cm}^2\,\mathrm{g}^{-1}$
γ	lumped kinetic parameter, $\mathrm{E}^{-1/2}\,\mathrm{cm}^{3/2}\,\mathrm{s}^{1/2}$
δ_n	nth eigenvalue of an ordinary differential equation
κ_{λ}	absorption coefficient of the medium, cm^{-1}
$\kappa^{*}_{\lambda,\mathrm{catal}}$	specific absorption coefficient of the catalyst, $\mathrm{cm}^2\,\mathrm{g}^{-1}$
$\kappa^{*}_{\lambda,\mathrm{dye}}$	specific absorption coefficient of the dye, $\mathrm{cm}^2\,\mathrm{g}^{-1}$
λ	wavelength, μm
θ	polar angle inside tubular reaction volume, rad

θ_s	scattering angle, rad
ρ	reflectance function of a surface
ρ_i	ith moment of the reflectance function
ρ_p	reflectance of the polyethylene wall
ρ_g	reflectance of the glass wall
σ_λ	scattering coefficient of the medium, cm^{-1}
$\sigma^*_{\lambda,catal}$	specific scattering coefficient of the catalyst, $cm^2\ g^{-1}$
τ	surface transmittance function
φ	polar angle around receiver tube, m
Φ_λ	scattering phase function
$\Phi_{HG,\lambda}$	Henyey–Greenstein scattering phase function
ω_λ	scattering albedo
Ω	solid angle, sr

ABBREVIATIONS

CPC	compound parabolic collector
DOM	discrete ordinates method
LVRPA	local volumetric rate of photon absorption
MCM	Monte Carlo method
RTE	radiative transfer equation
TC	tubular collector
UV	ultraviolet
VTC	V-trough collector

REFERENCES

Alfano, O.M., Bahnemann, D., Cassano, A.E., Dillert, R., and Goslich, R. *Catal. Today* **58**, 199 (2000).

Alfano, O.M., Cabrera, M.I., and Cassano, A.E. *J. Catal.* **172**, 370 (1997).

Alpert, D.J., Sprung, J.L., Pacheco, J.E., Prairie, M.R., Reilly, H.E., Milne, T.A., and Nimlos, M.R. *Sol. Energy Mater.* **24**, 594 (1991).

Arancibia-Bulnes, C.A., Bandala, E.R., and Estrada, C.A. *Catal. Today* **76**, 149 (2002a).

Arancibia-Bulnes, C.A., Bandala, E.R., and Estrada, C.A. Radiation absorption in parabolic trough and CPC solar photocatalytic reactors. *in* A. Steinfeld (Ed.), "Proceedings of the 11th Solar PACES Symposium on Concentrated Solar Power and Chemical Energy Technologies", Sept. 4–6, 2001, Zurich, Paul Scherrer Institut, Zurich (2002b), p. 445.

Arancibia-Bulnes, C.A., and Cuevas, S.A. *Sol. Energy* **76**, 615 (2004).

Arancibia-Bulnes, C.A., and Ruiz-Suárez, J.C. *Appl. Opt.* **38**, 1877 (1999).

Bahnemann, D. *Sol. Energy* **77**, 445 (2004).

Bahnemann, D.W., Bockelmann, D., and Goslich, R. *Sol. Energy Mater.* **24**, 175 (1991).

Ballari, M.M., Brandi, R., Alfano, O., and Cassano, A. *Chem. Eng. J.* **136**, 50 (2008).

Bandala, E.R., Gelover, S., Leal, M.T., Arancibia-Bulnes, C., Jiménez, A., and Estrada, C.A. *Catal. Today* **76**, 189 (2002).

Bandala, E.R., Arancibia-Bulnes, C.A., Orozco, S.L., and Estrada, C.A. *Sol. Energy* **77**, 503 (2004).

Bandala, E.R., and Estrada, C. *J. Sol. Energy Eng.* **129**, 22 (2007).

Bedford, J., Klausner, J.F., Goswami, D.Y., and Schanze, K.S. *J. Sol. Energy Eng.* **116**, 8 (1994).
Blanco, J., Malato, S., Fernandez, P., Vidal, A., Morales, A., Trincado, P., Oliveira, J.C., Minero, C., Musci, M., Casalle, C., Brunotte, M., Tratzky, S., Dischinger, N., Funken, K.-H., Sattler, C., Vincent, M., Collares-Pereira, M., Mendes, J.F., and Rangel, C.M. *Sol. Energy* **67**, 317 (1999).
Blanco-Galvez, J., Fernández-Ibáñez, P., and Malato-Rodríguez, S. *J. Sol. Energy Eng.* **129**, 4 (2007).
Bockelmann, D., Weichgrebe, D., Goslich, R., and Bahnemann, D. *Sol. Energy Mater. Sol. Cells* **38**, 441. (1995).
Bohren, C.F., and Gilra, D.P. *J. Colloid Interface Sci.* **72**, 215 (1979).
Brandi, R.J., Alfano, O.M., and Cassano, A.E. *Chem. Eng. Sci.* **54**, 2817 (1999).
Brinker, J.C., and Scherer, G.W., "Sol-gel Science, The Physics and Chemistry of Sol-Gel Processing". Academic Press, New York (1990).
Brucato, A., Cassano, A.E., Grisafi, F., Montante, G., Rizzuti, L., and Vella, G. *AIChE J.* **52**, 3882 (2006).
Brucato, A., and Rizzuti, L. *Ind. Eng. Chem. Res.* **36**, 4748 (1997).
Bruscaglioni, P., Ismaelli, A., and Zaccanti, G. *Waves Random Media* **3**, 147 (1993).
Cabrera, M.I., Alfano, O.M., and Cassano, A.E. *J. Phys. Chem.* **100**, 20043 (1996).
Carvalho, M.J., Collares-Pereira, M., Gordon, J.M., and Rabl, A., *Sol. Energy* **35**, 393 (1985).
Cassano, A.E., and Alfano, O.M. *Catal. Today* **58**, 167 (2000).
Chaves, J., and Collares Pereira, M. *J. Sol. Energy Eng.* **129**, 16 (2007).
Cuevas, S.A., Arancibia-Bulnes, C., and Serrano, B. *Int. J. Chem. Reactor Eng.* **5**, A58 (2007).
Cuevas, S.A., Villafán, H.I., and Arancibia-Bulnes, C.A. *in* "Proceedings of the XIII International Materials Research Congress". Academia Mexicana de Ciencia de Materiales, México (2004).
Curcó, D., Giménez, J., Addardak, A., Cervera-March, S., and Esplugas, S. *Catal. Today* **76**, 177 (2002).
Curcó, D., Malato, S., Blanco, J., and Giménez, J. *Sol. Energy Mater. Sol. Cells* **44**, 199 (1996a).
Curcó, D., Malato, S., Blanco, J., Giménez, J., and Marco, P. *Sol. Energy* **56**, 387 (1996b).
Diaz, J., Rodríguez, J., Ponce, S., Solís, J., and Estrada, W. *J. Sol. Energy Eng.* **129**, 94 (2007).
Gelover, S., Leal, T., Bandala, E.R., Román, A., Jimenez, A., and Estrada C. *Water Sci. Technol.* **42**, 101 (2000).
Gelover, S., Mondragón, P., and Jiménez, A. *J. Photochem. Photobiol. A: Chem.* **165**, 241 (2004).
Gernjak, W., Maldonado, M.I., Malato, S., Cáceres, J., Krutzler, T., Glaser, A., and Bauer R. *Sol. Energy* **77**, 567 (2004).
Giménez, J., Curcó, D., Queral, M.A. *Catal. Today* **54**, 229 (1999).
Goslich, R., Dillert, R., and Bahnemann, D. *Water Sci. Technol.* **35**, 137 (1997).
Goswami, D.Y. Engineering of the solar photocatalytic detoxification and disinfection processes. *in* K.W. Boer (Ed.), "Advances in Solar Energy, Vol. 10". American Solar Energy Society, Boulder (1995), p 165.
Goswami, D.Y. *J. Sol. Energy Eng.* **119**, 101 (1997).
Goswami, D.Y., Kreith, F., and Kreider, J.F., "Principles of Solar engineering, 2nd Edn". Taylor & Francis, Philadelphia (2000), Chap. 10.
Gryglik, D., Miller, J.S., and Ledakowickz, S. *Sol. Energy* **77**, 615 (2004).
Guillard, C., Disdier, J., Monnet, C., Dussaud, J., Malato, S., Blanco, J., Maldonado, M.I., and Herrmann, J.-M. *Appl. Catal. B: Environ.* **46**, 319 (2003).
Hulstrom, R., Bird, R., and Riordan, C. *Sol. Cells* **15**, 365 (1985).
Ishimaru, A. "Wave Propagation and Scattering in Random Media". Oxford University Press, Oxford (1997).
Jetter, S.M. *Sol. Energy* **37**, 335 (1986).
Jetter, S.M. *Sol. Energy* **39**, 11(1987).
Jiménez, A.E., Estrada, C.A., Cota, A.D., and Román, A. *Sol. Energy Mater. Sol. Cells* **60**, 85 (2000).

Jiménez, A.E., and Salgado, I. in preparation (2008).
Jiménez González, A.E., and Gelover Santiago, S. *Semicond. Sci. Technol.* **22**, 709 (2007).
Jiménez-González, A.E., Salgado-Tránsito, I., Payán-Martínez, L.F., and Ramón-García, M.L., submitted to *J. Photochem. Photobiol. A: Chem.* (2009).
Lebedev, A.N., Gartz, M., Kreibig, U., and Stenzel, O. *Euro. Phys. J. D* **6**, 365 (1999).
Li Puma, G., and Brucato, A. *Catal. Today* **122**, 78 (2007).
Li Puma, G., Khor, J.N., and Brucato, A. *Environ. Sci. Technol.* **38**, 3737 (2004).
Li Puma, G., and Yue, P.L. *Chem. Eng. Sci.* **58**, 2269 (2003).
Mahan, J.R. "Radiation Heat Transfer: A Statistical Approach". Wiley, New York (2002).
Malato, S., Blanco, J., Richter, C., Curco, D., and Giménez, J. *Water Sci. Technol.* **35**, 157 (1997).
Malato, S., Blanco, J., Alarcón, D.C., Maldonado, M.I., Fernández-Ibáñez, P., and Gernjak, W. *Catal. Today* **122**, 137 (2007).
Malato Rodríguez, S., Blanco Gálvez, J., Maldonado Rubio, M.I., Fernández Ibañez, P., Alarcón Padilla, D., Collares Pereira, M., Farinha Mendes, J., Correia de Oliveira, J. *Sol. Energy* **77**, 513 (2004).
Marshak, R.E. *Phys. Rev.* **71**, 443 (1947).
McLoughlin, O.A., Fernández Ibañez, P., Gernjak, W., Malato Rodríguez, S., and Gill, L.W. *Sol. Energy* **77**, 625 (2004a).
McLoughlin, O.A., Kehoe, S.C., McGuigan, K.G., Duffy, E.F., Al Touati, F., Gernjak, W., Oller Abedrola, I., Malato Roidríguez, S., Gill, L.W. *Sol. Energy* **77**, 657 (2004b).
Meichtry, J.M., Lin, H.J., de la Fuente, L., Levy, I.K., Gautier, E.A., Blesa, M.A., Litter, M.I. *J. Sol. Energy Eng.* **129**, 119 (2007).
Minero, C., Pelizzetti, E., Malato, S., and Blanco, J. *Chemosphere* **26**, 2103 (1993).
Modest, M.F. "Radiative Heat Transfer", 2nd Edn. Academic Press, New York (2003).
Mundy, W.C., Roux, J.A., and Smith, A.M. *J. Opt. Soc. Am.* **64**, 1593 (1974).
Navntoft, C., Araujo, P., Litter, M.I., Apella, M.C., Fernández, D., Puchulu, M.E., Hidalgo, M.V., and Blesa, M.A. *J. Solar Energy Eng.* **129**, 127 (2007).
Okamoto, K., Yamamoto, Y., Tanaka, H., and Itaja, A. *Bull. Chem. Soc. Jpn* **58**, 2023 (1985).
Olver, F.W.J. *in* M. Abramowitz, I.A. Stegun (Eds.), "Handbook of Mathematical Functions". Dover, New York (1972).
Oyama, T., Aoshima, A., Horikoshi, S., Hidaka, H., Zhao, J., and Serpone, N. *Sol. Energy* **77**, 525 (2004).
Pasquali, M., Santarelli, F., Porter, J.F., and Yue, P.-L., *AIChE J.* **42**, 532 (1996).
Pichat, P., Vannier, S., Dussaud, J., and Rubis, J.-P. *Sol. Energy* **77**, 533 (2004).
Rabl, A. *Sol. Energy* **18**, 112 (1976).
Rabl, A. "Active Solar Collectors and their Applications". Oxford University Press, New York (1985).
Román Rodríguez, A. Master's degree Thesis, UNAM. México (in Spanish) (2001).
Romero, R.L., Alfano, O.M., and Cassano, A.E. *Ind. Eng. Chem. Res.* **42**, 2479 (2003).
Salaices, M., Serrano, B., and de Lasa, H.I. *Ind. Eng. Chem. Res.* **40**, 5455 (2001).
Salaices, M., Serrano, B., and de Lasa, H.I. *Chem. Eng. J.* **40**, 219 (2002).
Satuf, M.L., Brandi, R.J., Cassano, A.E., and Alfano, O.M. *Ind. Eng. Chem. Res.* **44**, 6643 (2005).
Spott, T., and Svaasand, L.O. *Appl. Opt.* **39**, 6453 (2000).
Sudiarta, I.W., and Chylek, P. *J. Quant. Spectrosc. Radiat. Transfer* **18**, 709 (2001).
Trujillo, F.J., Safinski, T., and Adesina, A.A. *J. Sol. Energy Eng.* **129**, 27 (2007).
Turchi, C.S., and Ollis, D.F. *J. Catal.* **122**, 178 (1990).
van Well, M., Dillert, R.H.G., Bahnemann, D.W., Benz, V.W., and Mueller, M.A. *J. Sol. Energy Eng.* **119**, 114 (1997).
Villafán-Vidales, H.I., Cuevas, S.A., and Arancibia-Bulnes, C.A. *J. Sol. Energy Eng.* **129**, 87(2007).
Winston, R., Miñano, J.C., and Benítez, P. "Nonimaging Optics". Elsevier Academic Press, Amsterdam (2005).
Yokota, T., Cesur, S., Suzuki, H., Baba, H., and Takahata, Y. *J. Chem. Eng. Jpn.* **32**, 314 (1999).